

MOUSE RETINAL IMAGING

Moving the demonstrated OCT phase contrast techniques into retinal imaging, the choice is whether to use human subjects or another animal model which will provide a similar retinal environment. All of the acquisition methods do not produce any more risk to the vision of a human patient than standard OCT imaging, which has been determined safe for given illumination levels determined by the American National Standards Institute (ANSI). The choice of retinal imaging subject becomes a matter of preference once there are no safety concerns.

While the contrast techniques are still in the developmental stages, mouse imaging has several advantages. With mouse animal models, a large population of subjects can be developed for imaging in a short amount of time, including numerous genetic strains to produce abnormalities in the structures of interest. With the short lifespan compared to humans, disease progression within a mouse will be much faster and easier to monitor experimentally. Unlike human subjects, histology of the imaged mouse subjects can be produced when necessary for comparisons to observed phenomena. Once all of the analysis techniques have been developed for retinal imaging in the mouse, they can be adapted for use in human retinal imaging systems.

5.1 Human Retinal OCT Imaging Explained

Retinal imaging with human subjects utilizes the patient's own eye as the final focusing lens of the imaging system, with all of its limitations. The transverse scanning of the imaging light pivots about the center of the eye lens, limiting aberrations introduced while scanning and minimizing clipping introduced by the pupil.

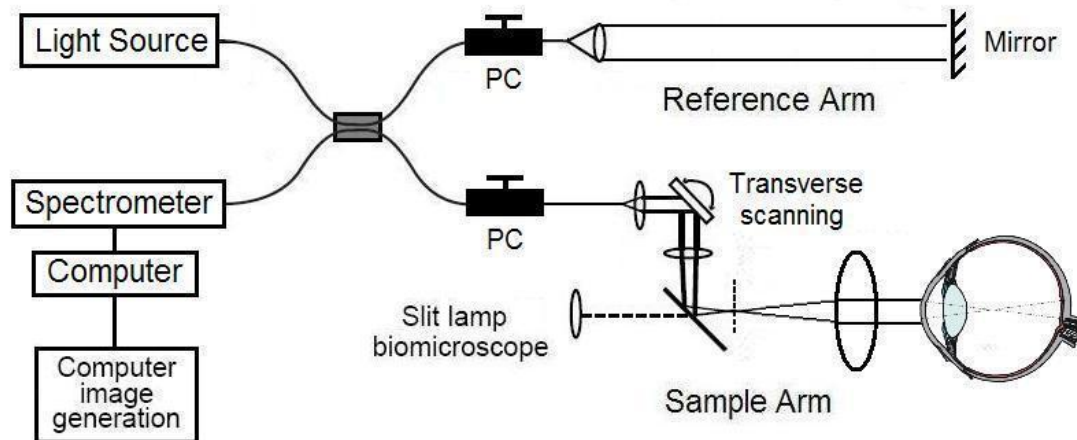


Figure 5.1: Schematic of fiber optic human retinal SDOCT system. PC: polarization controller. The slit lamp biomicroscope combines the OCT imaging with a fundus camera system.

One form of the retinal imaging sample arm of the interferometer is called a slit lamp biomicroscope, which is a combination of the confocal transverse scanning of the OCT interferometer as well as a slit lamp setup for creating a full field fundus image. The Stratus OCT retinal imaging system (Carl Zeiss Meditec) uses this type of sample arm to acquire simultaneous OCT and fundus images. The sensitivity of the fundus camera in this setup allows for visualization of the transverse scan location of the OCT image in addition to the fundus reflectivity.

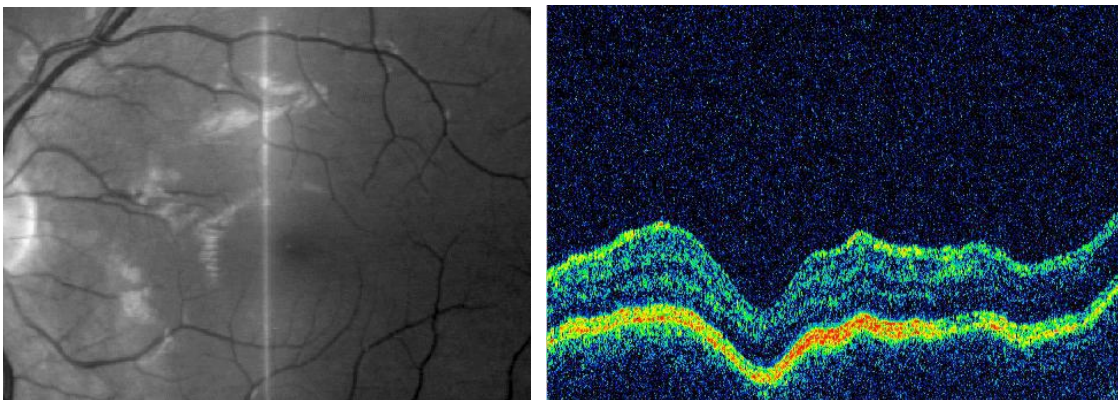


Figure 5.2: Fundus image and OCT intensity image acquired simultaneously with retinal Stratus OCT imaging system created by Carl Zeiss Meditec. The fundus image can visualize a fraction of the reflected OCT light source, demonstrating the transverse location of the corresponding OCT scan (vertical line on fundus image).

The experimental SDOCT system uses a slit lamp biomicroscope from a Stratus OCT system, adapted for use in mouse retinal imaging. To adapt the scanning system intended for human eyes to be able to image mouse eyes, the differences between imaging the two types must be understood.

5.2 Differences between Human and Mouse Eye Imaging

The major difference between human and mouse eyes are the size of the eyes. Human eyes have a typical length from the front of the cornea to the retina of 25 mm. Mouse eyes have a length of around 3 mm, depending on the age of the animal. This eye length determines the focal length of the lens, and with the maximum pupil diameter limits the minimum transverse resolution possible for the aberration-free retinal imaging case.



Figure 5.3: Photograph of mouse, demonstrating an eye length of approximately 3mm for this case.

As in the human imaging case, mouse eyes cannot be considered aberration-free in general. Mouse eyes contain multiple aberrations and are typically myopic (eye length is too long for the eye's focus length), limiting the resolution in the uncorrected case. While the lenses of the sample arm can be adjusted to compensate for some of the optical quality degradation, the result will still be aberration limited [1]. It is also important to maintain corneal hydration of the mouse eye to prevent optical focus and opacity changes which accompany dehydration [2].

To compensate for the majority of the aberrations and maintain hydration, the curvature of the mouse cornea must be altered while holding an aqueous solution at the surface of the cornea. A specially made contact lens can be created to compensate for the myopia of the mouse eyes, also reducing the aberrations introduced from the curvature of the cornea [3]. An easier approach is to remove the effect of cornea curvature by placing a flat cover glass in front of the eye while holding contact to the cornea with a saline solution [4]. With the majority of the focusing power removed from the eye itself, an external focusing lens can be added to replace the original focusing power. By relying on external focusing to image the mouse retina, the process of changing between different animal specimens becomes easier and less dependant on the individual optical quality of the eyes.

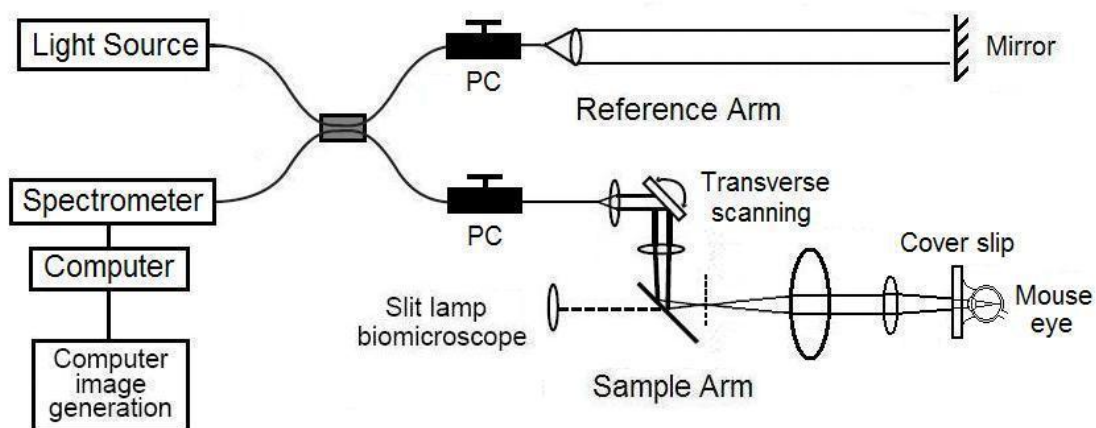


Figure 5.4: Schematic of fiber optic mouse retinal SDOCT system. PC: polarization controller. An additional focusing lens is added to the human retinal system to compensate for the focusing removed by the presence of the cover slip on the mouse eye.

Using the Stratus OCT scan optics, an additional focusing lens was used to allow imaging of the mouse retina. Using a cover slip to remove the focusing power of the mouse's eye, a focusing lens of focal length 18 mm would result in an estimated transverse resolution of approximately 14 μm . The depth of focus for this resolution would be approximately 370 μm , on the order of the retinal thickness in the mouse. For this retinal imaging system, the light source and the spectrometer can be utilized from the microscopy system described in Chapter 4. Due to different optical path lengths and dispersions of the sample interferometer arms for the two systems, different reference arms are required for each of the two imaging systems.

Aligning the human eye for retinal imaging is fairly simple with the help of an external fixation target which allows the patient to align their position to be able to visualize the target. The mouse, which cannot be aligned using a fixation target, requires additional positional alignment to align the retina for imaging. Five degrees of freedom are required to allow all range of alignments for imaging: three translational directions as well as rotation about the x-axis and the y-axis, where the z-axis is defined by the optical imaging direction. Due to the flexibility of the transverse scanning in the system, rotation about the z-axis is not required.

The average mouse will not remain stationary during this optical alignment and imaging, necessitating the use of anesthetic to put the animal to sleep. The lack of blinking experienced by the mouse during the anesthetic can be a main source of corneal dehydration discussed earlier. The anesthesia solution used for mice in the experiment was a combination ketamine/xylazine mixture, containing 0.1mL Xylaject (xylazine hydrochloride injection), 0.3 mL Ketaject (ketamine hydrochloride injection), and 4 mL sterile phosphate buffer solution (PBS).

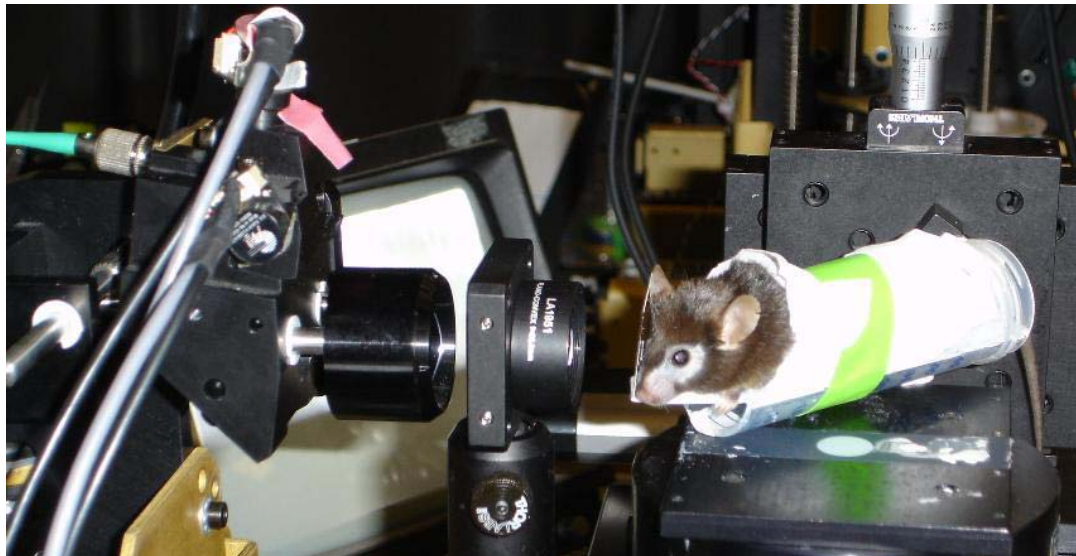


Figure 5.5: Photograph of sample arm of interferometer for mouse retinal system. Mouse is secured in holder after anesthetic with a cover slip attached to the cornea of the eye with a saline solution. The holder provides five degrees of freedom of alignment for the mouse relative to the imaging optics.

5.3 Aligning Retinal SDOCT Images

With the sample arm set up with external focusing, the maximum scan range of the retina is limited by the size of the pupil. Similar to ophthalmologic diagnosis for human eyes, a chemical was used to dilate the pupil and temporarily fix the accommodation of the lens, facilitating the imaging procedure. For the experiment, two drops of 1% tropicamide were used to dilate the pupils of each eye used for OCT imaging. Fundus camera images were taken before the chemical was applied and after full dilation, with both images acquired without a cover glass on top of the cornea.

With a cover glass placed on the eye with a saline buffer solution, the fundus image can be focused to visualize the retina. The optic nerve head and some of the vasculature can be seen with this image, but the image quality depends on the camera and the image parameters. With the ability of the fundus camera to visualize the scan line of the OCT light source, the camera can also act as a coarse alignment of the transverse position of the SDOCT images.

In the experimental system, the optimal focus for the retinal fundus image did not match the optimal alignment of the SDOCT images. To adjust the SDOCT image focus from the optimal fundus focus, there are three elements that can be adjusted in the system: the final two lenses of the sample arm and the depth position of the mouse. By aligning the optics for optimal OCT coupling of a static paper sample, the optical alignment of the lenses was determined. With these positions, only the depth position of the mouse eye was altered to maximize coupling from the retina.

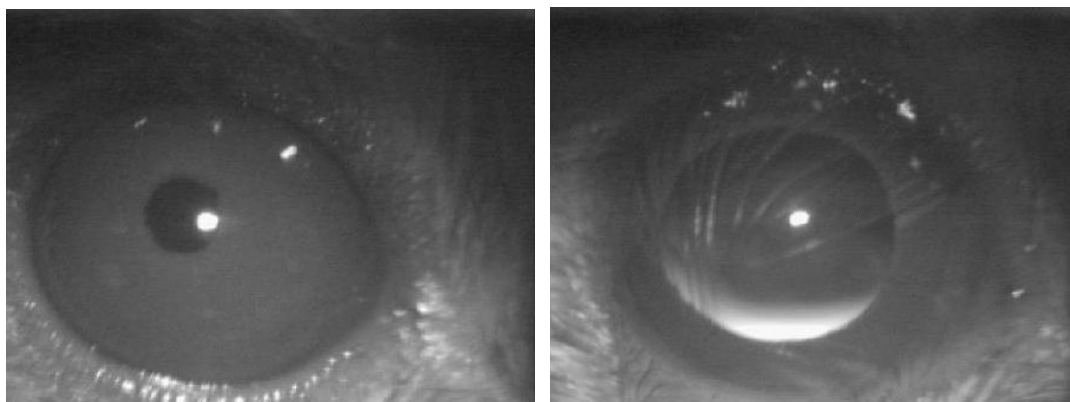


Figure 5.6: Fundus camera images demonstrating the dilation of pupils with application of tropicamide. The undilated pupil (left) is substantially smaller than the dilated case (right). Eye lashes of the mouse are present in front of the cornea on the dilated pupil image. No cover glass is used in these images.

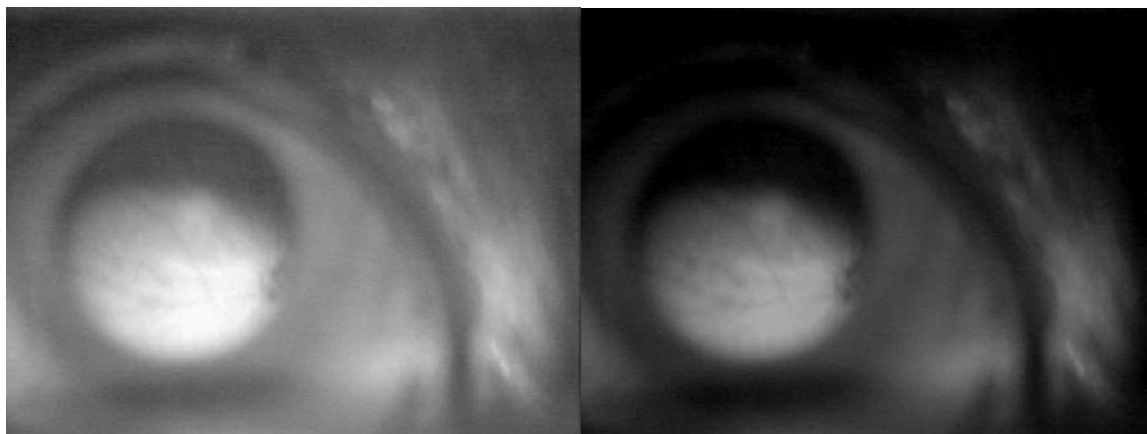


Figure 5.7: Fundus camera image after application of cover slip. Optic nerve head and some vasculature can be visualized in the retina. Two different image contrast parameters are presented to assist with visualization.

Retinal B-scan images were maximized through a series of alignments. Near the optimum sample focus, shadowing from the blood vessel absorption becomes more prominent. At the optimal focus, the reflection from the top of the surface retinal blood vessels is maximized. To maximize the interference signal, the polarization controllers were adjusted for each of the interferometer arms. The important factor to note during alignment is the reference arm coupling changes over extended changes in path length. As the sample position changes to deeper image locations (further away from the equal path length position of the reference arm), the signal will drop due to the SNR drop over depth. If the reference arm coupling decreases as the image is re-aligned back to the equal path length position, the image will appear lower in intensity than expected for a given coupling. Constant reference arm power during the alignment process is crucial for identifying the optimal sample coupling location.

The transverse scan length of the OCT imaging in the mouse retina can only be approximated due to the uncertainty of the contribution from the optics of the mouse eye on the imaging system. With the variability introduced by the alignment of the external optics to improve focusing, image feature sizes and previous images are used to help approximate the transverse scan length on the retina.

5.4 Phase Contrast Imaging

To determine if more system optimization is required before phase contrast analysis is performed, a sample B-scan created using the retinal imaging system is compared to one of the limited amount of high resolution SDOCT images published for the mouse retina [4]. The B-scan image from the previously published work identifies the different layered regions of the retina over the entire depth: the inner plexiform layer (IPL), inner nuclear layer (INL), outer plexiform layer (OPL), outer nuclear layer (ONL), photoreceptor inner segments (PR IS) and outer segments (PR OS), retinal pigment epithelium (RPE), and choroid (CH).

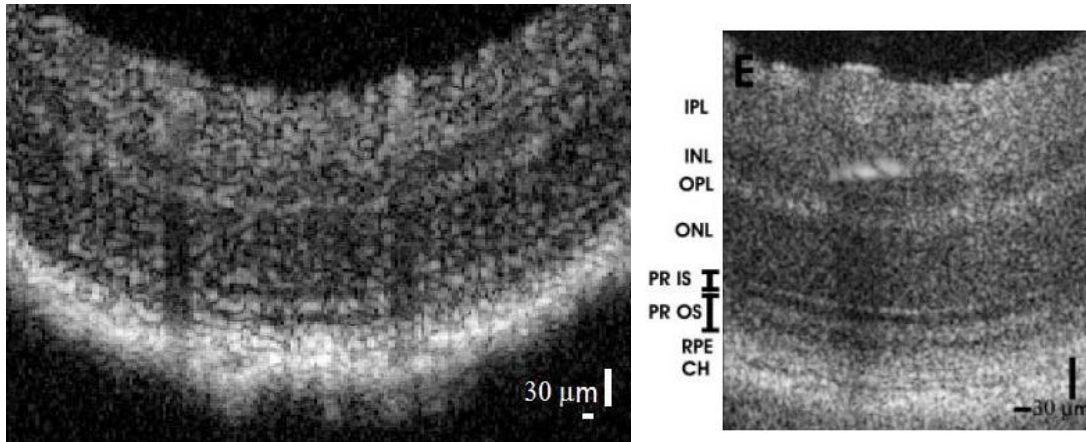


Figure 5.8: OCT intensity B-scan comparison between experimental retinal imaging system (left) and previously published results (right) [4]. The experimental B-scan is composed of 200 A-scans acquired over a scan length of approximately 2mm. Published results demonstrate a B-scan composed of 600 A-scans acquired over approximately 600 μm . Similar image scales are presented to improve comparison.

Comparing the images between the experimental system and previously published data, there are differences between the image parameters. The experimental system has an axial resolution of 6 μm in tissue, while the published system has an axial system of approximately 2 μm in tissue (2.8 μm in air). The published B-scan also has a higher density of A-scans within the image: it uses 600 A-scans over approximately 600 μm while the B-scan from the experimental system uses 200 A-scans over approximately 2 mm.

As expected, both images demonstrate a mouse retinal thickness of approximately 300 μm . The separation of the retinal layers can be observed in both images, but the published image appears to have improved visualization of the layers over regions of the image. This visualization improvement is likely due to the higher sampling density, which is 1 μm between A-scans, compared to the 10 μm spacing used in the experimental image. The increased density not only reduces the speckle observed in the image, but it reduces the SNR loss experienced while scanning over tilted correlated scatterers as explained in Chapter 3.2. The only portion of the retinal image which appears to depend on the axial resolution difference between images is the separation of the RPE and choroidal layers of the published image, which is not evident in the experimental image. With general

consistency between the two images, it is concluded that the performance of the experimental system is adequate for comparison to previously demonstrated systems.

Due to the thin structure of the retina, visualization is improved by using different scaling on the transverse and axial directions of the image. Unless otherwise stated, the presented images within this chapter uses a relative scaling of 3:1 to expand the axial direction of the image and make the retina appear thicker as demonstrated in Figure 5.8.

5.4.1 MB-scan

With the amount of statistics available to be analyzed, the first phase contrast acquisition method for the retina is the MB-scan. Using a buffered acquisition for a total of 1.6 s, 200 A-scans were acquired for each of 200 transverse locations along the retina. From the averaged OCT intensity image, it is obvious that the situation has changed from the zebrafish imaging of Chapter 4. The averaged intensity image shows the retinal layered structure, which becomes blurred in regions which can be assumed are associated with flow. The Doppler flow image is calculated for the case of 5 phase change averages with a scale of ± 2 radians, which is equivalent to an axial flow rate of ± 2.5 mm/s. On this image, large axial flow is observed in the same transverse locations as the blurred regions of the intensity image.

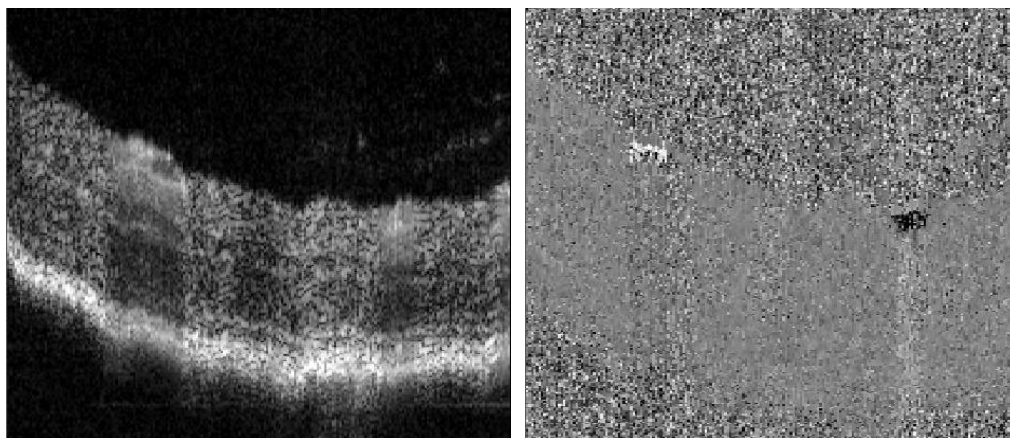


Figure 5.9 a): MB-scan averaged intensity image (left) and Doppler flow image from successive phase changes using 5 averages (right). The Doppler flow image does not use any thresholds and has a scale which corresponds to ± 2.5 mm/s.

While the fast flows are easily observable in the Doppler image, the identification of slower flow is important for the visualization of the smallest vessels. There are two main methods to improve the flow visualization with the Doppler flow technique: averaging more to reduce phase noise, and using larger time separations of phase changes to observe slower flow. The minimum axial velocity that can be visualized is determined by the phase noise divided by the time between phase measurements. One of the consequences of the increased time separation is the reduction of the maximum axial flow that can be measured before phase wrapping takes effect.

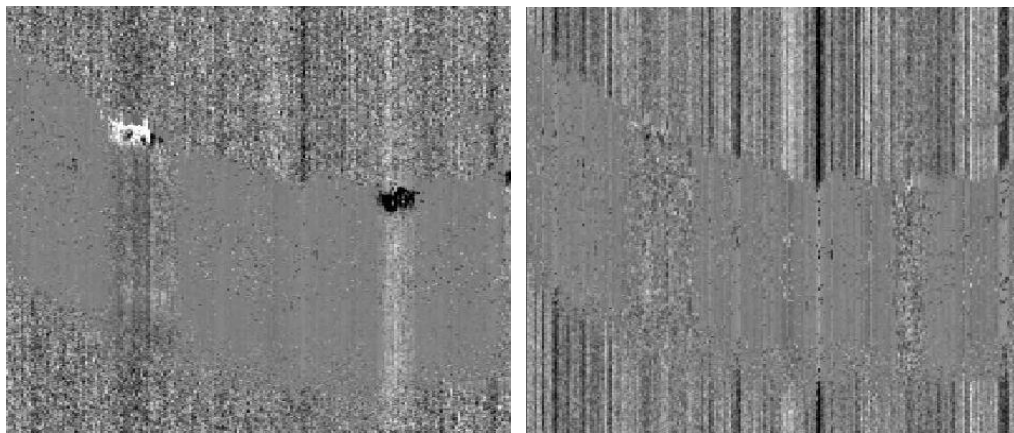


Figure 5.9 b): MB-scan Doppler flow images created using 50 averages for the phase change time separations of by 40 μs (left) and 200 μs (right). The axial flow scale on the images are ± 1.25 mm/s (left) and ± 2.5 mm/s (right), with no thresholds applied to either image.

By increasing the statistics of the averaging from 5 to 50, the phase noise of the Doppler image is expected to reduce by a factor of $10^{1/2}$. To take advantage of the reduced noise, the scale of the flow image is reduced to ± 1 radians = ± 1.25 mm/s. It is unclear whether additional flow locations can be observed even with this improved noise situation. Using the time separation of 200 μs , 5 times the acquisition time between successive A-scan acquisition, the Doppler flow image is calculated with 50 averages as well using a scale of ± 2 radians. As with the increased statistics case, there are no obvious new flow locations associated with this new analysis method. With this method, the phase wrapping on the fast flows caused a decreased visualization without any demonstrated benefits. It should be

noted that the lines of contrast on the Doppler images are artifacts located on the noise pixels caused by the bulk axial motion removed during the acquisition time at each transverse location.

To work on the phase variance contrast, the phase variance was calculated for time separation of $40\ \mu\text{s}$, previously considered to be a good approximation of the SNR-limited phase noise of the image. With the calculation of bulk motion removal but without using any thresholds or numerical phase removal, the phase variance was plotted for the cases of 10 phase changes and 200 phase changes.

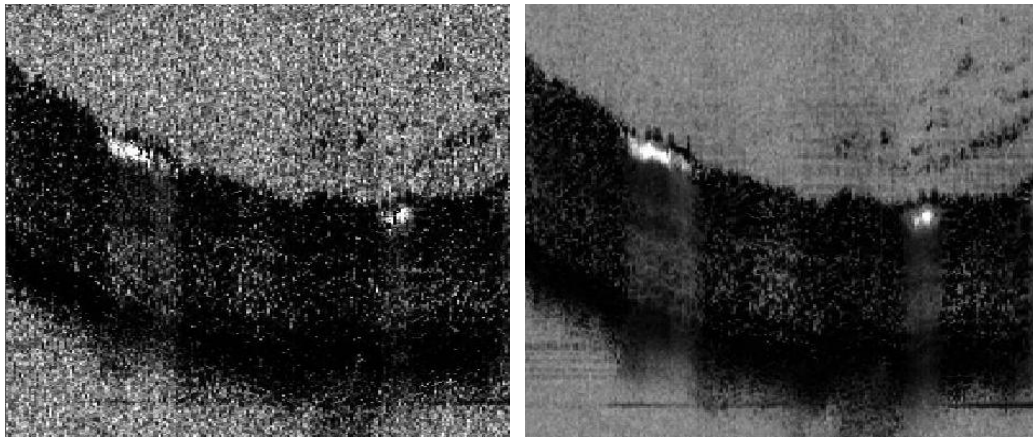


Figure 5.10: MB-scan phase variance images for phase measurements from successive A-scans with a time separation is $40\ \mu\text{s}$. The total number of phase changes used for the variance calculation at each transverse location is 10 (left) and 200 (right). The scale on these images is 0 to 6 radians².

One of the major anomalies of these images is the scale used to image the phase variance. The maximum of these images corresponds to 6 radians², twice as large as used for any previously demonstrated phase variance contrast images. Theoretically, a purely random phase would only produce a phase variance of approximately 3.3 radians², suggesting that the large variance contrast observed might be an artifact of the phase analysis procedure for this case. As discussed in Chapter 4.3, an axial motion of approximately π radians with a variance will result in a very large variance calculation while the mean value is miscalculated lower than expected. Further data is required to analyze the phenomena further.

From the phase variance calculations, it is clear that the sequential phase change situation is not properly representative of only the phase error of the image. To calculate the phase variance contrast images using the MB-scan, a numerical estimate identical to the BM-scan contrast method is applied for phase noise removal. Phase variance contrast is plotted for a range in phase change time separations from $40 \mu\text{s}$ to $320 \mu\text{s}$, with each case of time separation larger than $40 \mu\text{s}$ using the same statistics of 40 phase changes to calculate the phase variance. The scale used for all of the contrast images was 0 to 3 radians².

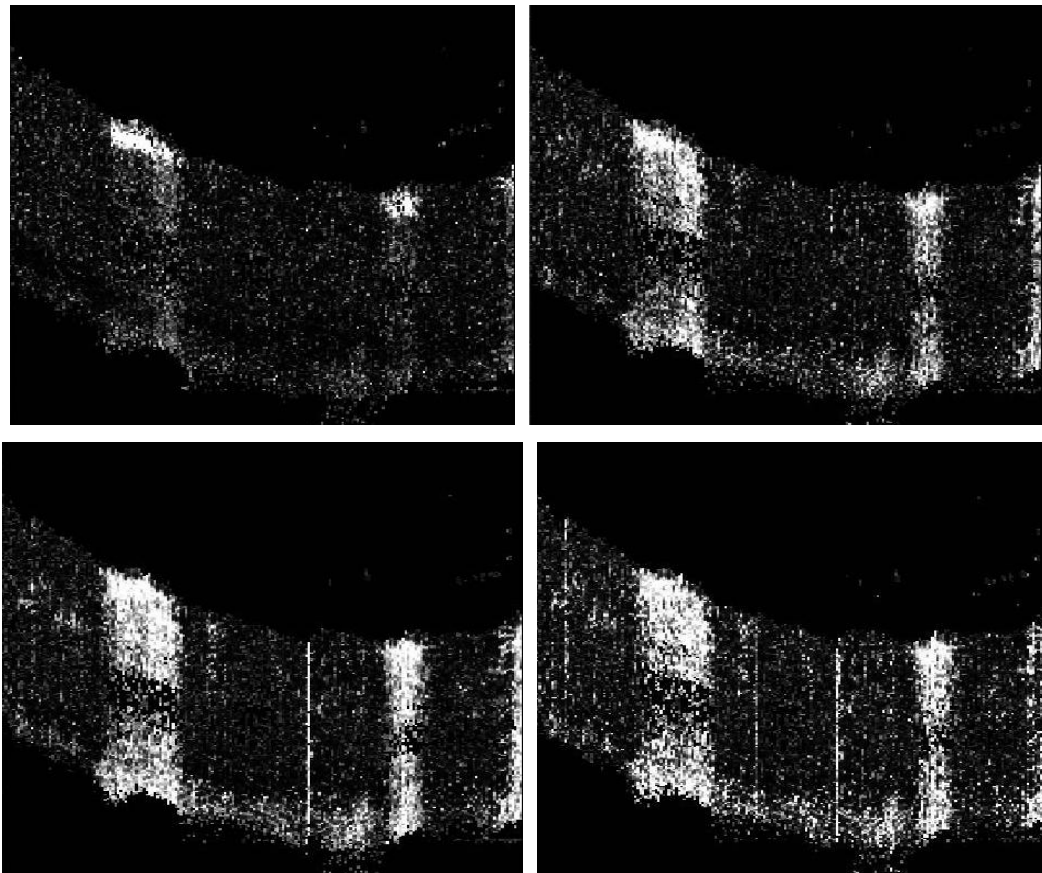


Figure 5.11: MB-scan phase variance contrast for the cases of $40 \mu\text{s}$ time separation with 10 phase changes (upper left) and for $160 \mu\text{s}$ (upper right), $240 \mu\text{s}$ (lower left) and $320 \mu\text{s}$ (lower right) time separation of phase changes using 40 phase changes to calculate variance.

From the demonstrated range of time separations of the phase contrast images, there are many trends that can be observed. With increased time separations comes an increase in the

calculated contrast shadowing below the large flowing vasculature. The shadowing across the entire depth can be observed even at the 160 μ s time separation case, which was not observable in the zebrafish tail at time separations as long as 1 ms. The motion contrast observed in the choroidal region of the mouse retina was also observed to increase with time separation of the phase changes. The increased time separation also results in an increased amount of noise within the contrast image. Very narrow vertical lines of contrast appear in the image, which increase in frequency with larger time separations. These anomalous artifacts could be due to transverse motion occurring during the M-scan at a given transverse location and the inability of the bulk motion calculation to remove these effects.

5.4.2 Single Scan Contrast Method

With the demonstrated phase variance contrast at very short time separations, another type of phase contrast acquisition method can be used to efficiently obtain 3D phase contrast information. Phase variance contrast images can be created from a single B-scan sampled very densely along the transverse scan direction [5]. Rather than waiting on a stationary transverse location for each M-scan used within the MB-scan, the measurements of phase over time with this technique are separated spatially by the transverse scanning as well as separated in time. This contrast method will be referred to as the single scan phase contrast method. By planning the scan density such that the transverse scan is much smaller than the transverse resolution of the system, the expected transverse scanning errors described in Chapter 3.3.4 can be minimized.

With the single scan phase contrast method, the short time separation of 40 μ s between phase measurements allows for the calculation of the Doppler axial flow as well as the phase contrast. For a B-scan containing 512 A-scans extended over approximately 2 mm for the mouse retina, contrast was determined using the phase from 5 transverse A-scans, all taken successively from each other. The plotted OCT intensity image was taken without any averaging. The Doppler flow was plotted using an image scale of ± 2 radians = ± 2.5 mm/s without any thresholds applied. The magnitude of the Doppler flow was plotted after

numerical removal of the estimated phase error and application of a threshold based on the intensity, with a scale of 0 to 2 radians. The phase variance was plotted without any numerical phase error removal or thresholds on the image. The first phase contrast image plots the phase variance after estimated phase error removal and thresholds applied. The second phase contrast image applies the same technique as well as using a median filter in both directions on the image. The scale used for the variance image is 0 to 3 radians² and for the phase contrast images is 0 to 2 radians². All of the contrast techniques use 5 total phase measurements to calculate the image at a given pixel.

To evaluate the capabilities of the single scan contrast method, the images with this method are compared to the images from the MB-scan data displayed in Figures 5.9, 5.10, and 5.11. The Doppler flow images show comparable flow amplitudes, suggesting that the retinal flow during both data acquisitions is consistent. While similar flow occurs within both situations, there is a discrepancy between the phase variance contrast images acquired for both cases. In the single scan phase contrast case, the phase variance of the flow regions was visible, but not as strong the MB-scan variance images. This discrepancy suggests that the large phase variance calculated in the MB-scan case was created by computational artifacts and phase wrapping of some of the flow data.

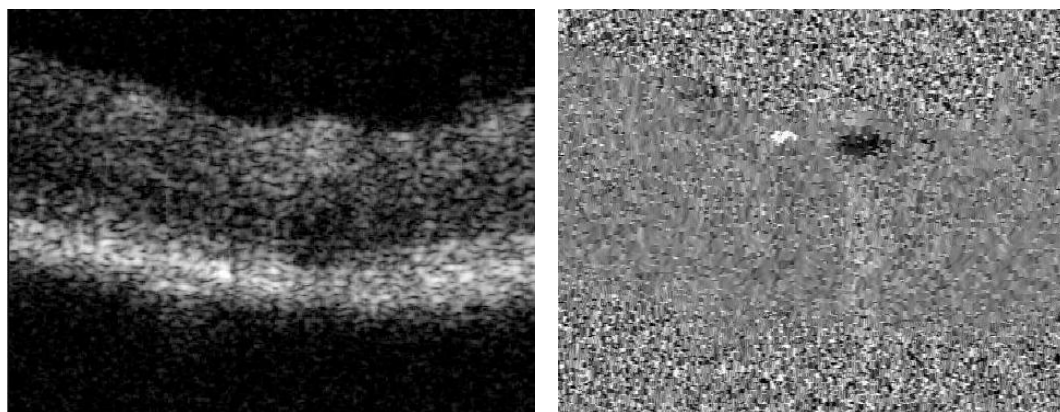


Figure 5.12 a): Single scan intensity image without averaging (left) compared to Doppler flow image over the same region. Doppler image uses 4 phase changes to calculate average flow, and is presented with a scale of ± 2.5 mm/s.

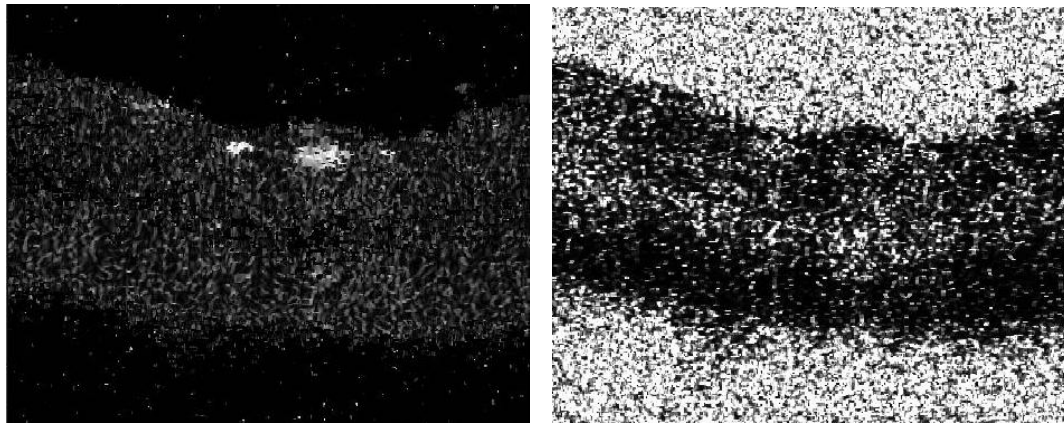


Figure 5.12 b): Magnitude of Doppler flow image with maximum scale of 2.5 mm/s (left), noise corrected using the phase variance noise measurement for the image (right) without any noise compensation or removal. Variance scale is 0 to 3 radians².

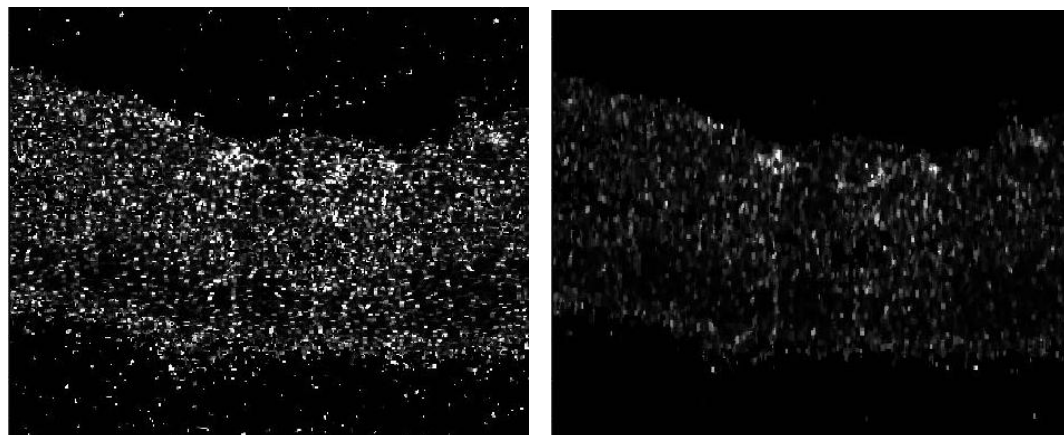


Figure 5.12 c): Phase variance contrast image presented before median filtering (left) and after it has been applied. Variance scale is 0 to 3 radians².

It is possible that the previously demonstrated single scan contrast was affected by the minimal density used in the B-scan. With 512 transverse pixels acquired over 2 mm each pixel separation is approximately 4 μm , resulting in phase contrast being calculated for data acquired over 20 μm transversely. Single scan phase contrast was acquired across 2 mm of retina for 4096 total A-scans, resulting in a transverse spacing between A-scans of approximately 0.5 μm . The phase contrast in this case was calculated over a transverse region of approximately 2.5 μm , much smaller than the expected transverse resolution of the imaging system. Only three images were calculated for this case: the averaged OCT

intensity image, the corrected magnitude of the Doppler flow calculation, and the phase variance contrast image for the region. The scale on the Doppler image was 0 to 1 radian and the phase variance contrast scale was 0 to 1 radians² in this case.

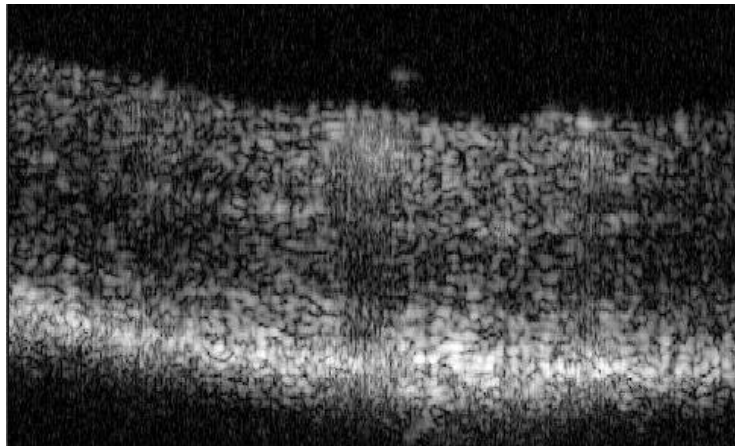


Figure 5.13 a): OCT intensity image from single scan acquisition of 4096 A-scans over approximately 2 mm, averaged over 5 neighbouring A-scans.

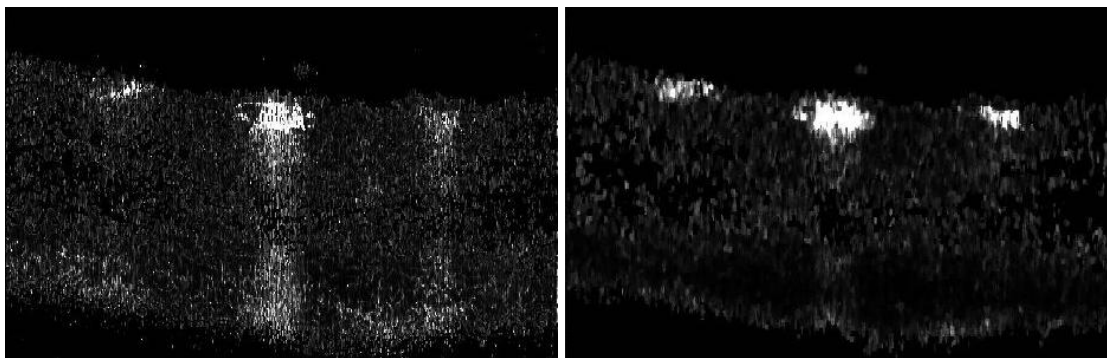


Figure 5.13 b): Single scan contrast images calculated from 4096 A-scans extending over approximately 2 mm. The magnitude of the Doppler image (left) and the phase variance contrast image (right) used numerical phase error removal and thresholds based on intensity. The image scales were 0 to 1 radian (left) and 0 to 1 radians² (right).

The averaged intensity image demonstrates some of the blurring below the flow regions within the image, but due to limited statistics the blurring is less substantial than the MB-scan image which uses 200 A-scans to perform the averaging. The motion contrast observed in this case appears different than the previous two demonstrated contrast

acquisitions. Two of the three flow regions which can be barely identified using the Doppler image can be clearly observed using the phase variance contrast method.

While the different forms of flow contrast observed for the retinal vessels can be investigated further, it is important to note that, for the short time separation contrast in the MB-scan and the single scan contrast method, there was no substantial motion contrast observed within the choroidal region of the retina. The goal of the contrast methods is the ability to visualize the earliest stages of choroidal neovascularization (CNV) in the human eye. If the choroidal vessels cannot be visualized, it is hard to argue that new vasculature growing from these methods will be able to be visualized.

5.4.3 BM-Scan

The BM-scan is used to image the mouse retina with the same parameters used for the majority of the zebrafish imaging: 200 transverse pixels, 5 B-scans per BM-scan and time between phase measurements $T = 10\text{ms}$. With a total of 1 GB of system memory and the chosen BM-scan parameters, a maximum of 51 BM-scans are acquired within one full buffered acquisition.

A BM-scan taken of the mouse retina over a section of the optic nerve head is presented with the averaged OCT intensity image. The phase variance was imaged using only a threshold based on the OCT intensity to remove the noise terms, demonstrating the requirement of not only the SNR-limited phase noise removal but the necessity of the median filtering on all of the contrast images. MB-scan phase variance contrast observed the appearance of non-negligible artifacts in the phase contrast image for time separations as short as $320\ \mu\text{s}$, much smaller than the 10 ms time separation of the BM-scan. The application of the median filtering into the phase contrast imaging analysis allows much clearer visualization of the flow regions within the image.

One very important note is that the BM-scan clearly observed motion contrast for the retinal vessels as well as motion located within the choroidal region of the retina. The only observation so far of the choroidal motion was using the MB-scan phase contrast images

for increasing time separation in Figure 5.11. Even in this case, the visualization was not as strong as with the BM-scan phase contrast image.

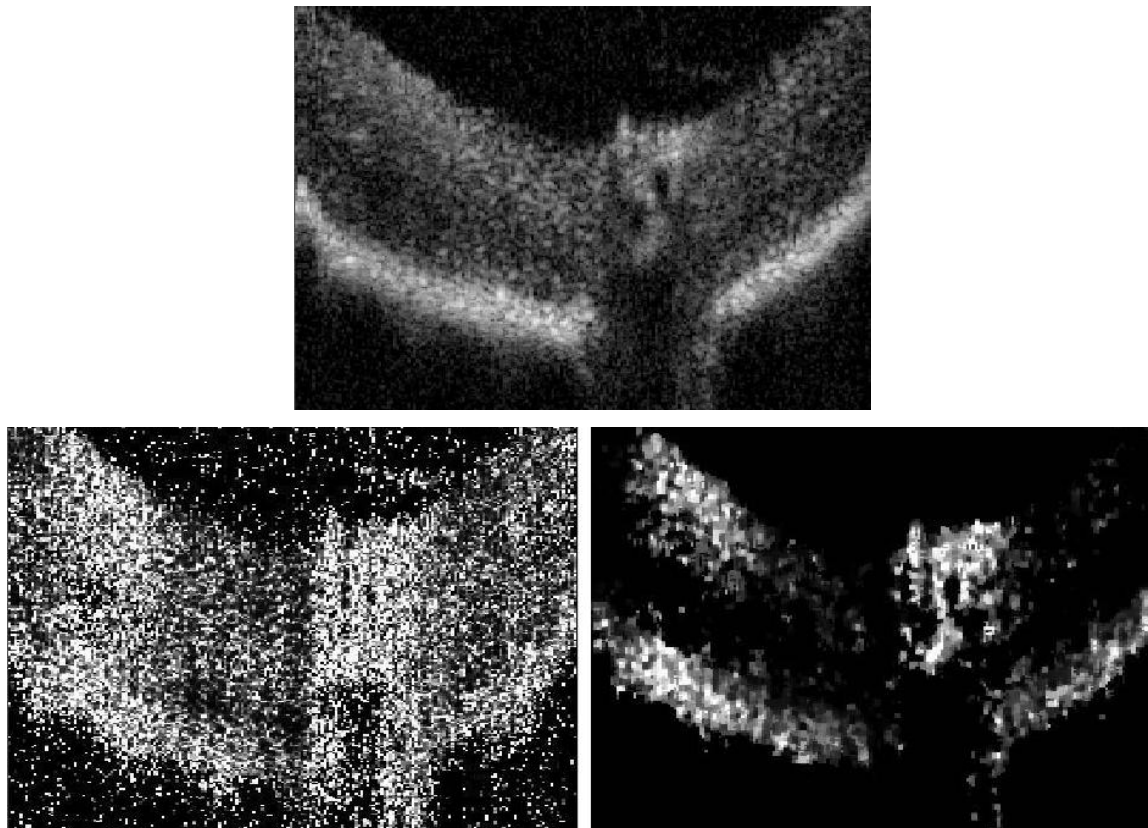


Figure 5.14: BM-scan images for mouse retina, including the averaged intensity image (top), the phase variance image (left) and the phase variance contrast image (right), which uses noise removal and median filtering. The variance images use the scale 0 to 3 radians².

5.4.4 Transverse Motion of Eye

For many stages of the retinal imaging, it was clear that the mouse was twitching during the imaging session. The impact to not only the alignment of the 3D data set, but also to the individual 2D phase contrast images needed to be determined. To demonstrate the alignment changes over time with the transverse motion, en face summation images were created by summing the linear form of the 3D OCT intensity data over the entire retina. OCT intensity data is presented in logarithmic form to improve the structural visualization of the image over the dynamic range of the reflections. By summing the linear form of the

intensity to create the en face image, the maximum reflection within the transverse location will dominate the resulting image. The en face image produced using this method is virtually identical to the image created by a scanning laser ophthalmoscope (SLO) discussed in Chapter 1.3.7.

The en face intensity images show the non-trivial transverse motion occurring during the 2.6s of image acquisition time. The motion observed within the image appears to be oscillatory in nature. With approximately nine oscillations in 2.6 s, this motion is at a frequency of ~ 3.5 Hz, very close to the expected heart rate of the mouse under anesthetic. If the oscillatory transverse motion creates motion artifacts within the phase contrast images, the en face contrast summation images will contain horizontal contrast lines which oscillate in intensity based on the effect of the transverse motion.

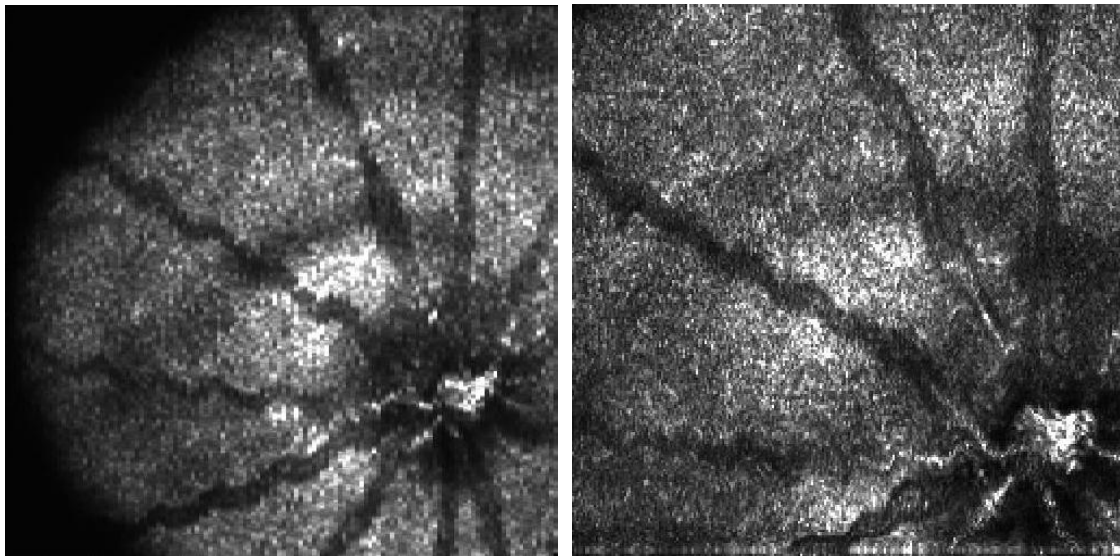


Figure 5.15: En face intensity summation images from two different acquisitions of 512 x 128 pixels (left) and 200 x 200 (right) over the mouse retina. Both images demonstrate the twitching in the mouse eye position over the 2.6 s acquisition time of images.

First, look at a 3D data set composed of single scan phase contrast images. With the short total time used for phase variance contrast (200 μ s), this method should not be affected much by the observed transverse motion. For a 1 GB memory buffer, 512 x 128 transverse locations can be acquired with this contrast method. Using the phase variance contrast data

to create the summation images, two different en face images were calculated. The first image summed the phase variance contrast over the entire depth of the retina, while the second image only summed the contrast terms which were greater than 2 radians^2 , trying to remove the effect of static terms which may have additional phase noise caused by the transverse motion scanning during the contrast calculation data. While the en face phase variance contrast images show the same expected oscillations in the vessel locations, there does not appear to be any major contrast variations caused by the transverse motion.

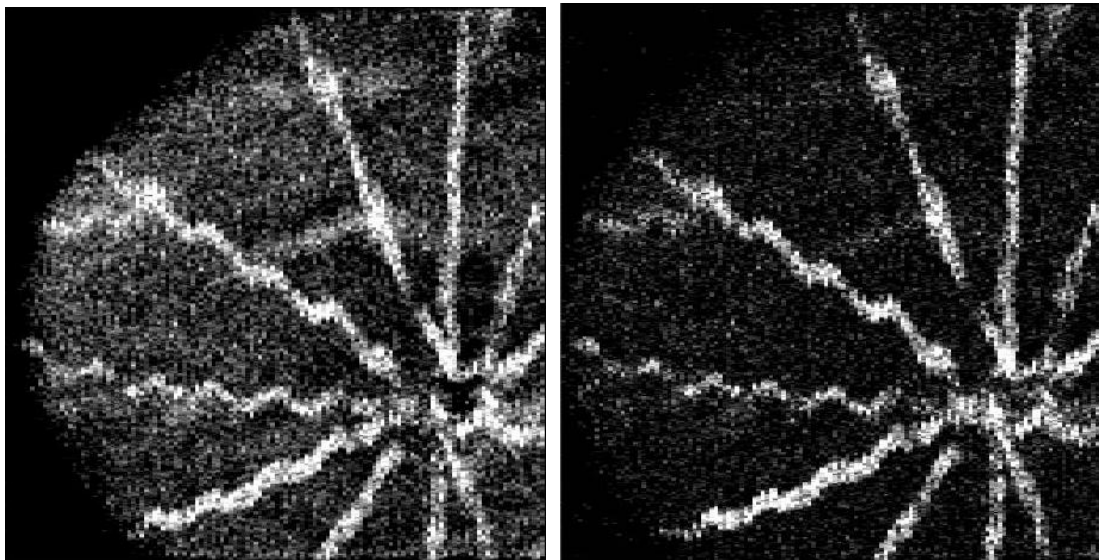


Figure 5.16: En face summation contrast images of phase variance contrast calculated using single scan contrast methods. The summations are performed over the full depth of the retina for the cases of all contrast data (left) and for only contrast data points $> 2 \text{ radians}^2$ (right). Image size is approximately $2 \text{ mm} \times 2 \text{ mm}$.

BM-scans are expected to be much more susceptible to artifacts caused by transverse motion because of the increased phase contrast time per pixel (50 ms) in this case. To observe the effect of the oscillatory motion on the summation contrast image, a buffered acquisition of BM-scans was taken over the same transverse scan location over time. The scan location was chosen to have several blood vessels for motion contrast as well as large regions of static retinal tissue, ideal to demonstrate the effect of this transverse motion on the motion contrast. There is a wide range of transverse motion measured within this data

set. The averaged OCT intensity image from a low noise BM-scan is compared to the phase variance contrast image for a high noise BM-case caused by transverse motion.

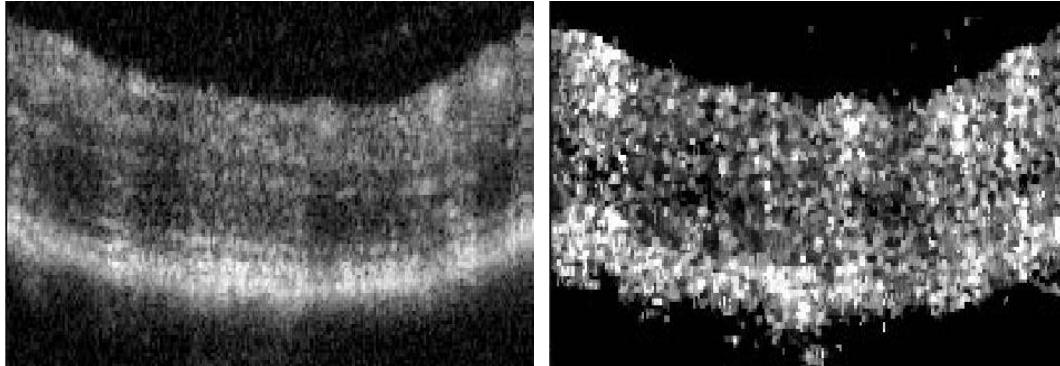


Figure 5.17: BM-scan data for retina undergoing transverse motion. The averaged intensity image (left) is calculated for a time point undergoing low transverse motion. The phase contrast image, after noise removal and median filtering, is taken from a time point experiencing large transverse motion.

The main approach to deal with this additional motion noise is to treat it as another noise source that needs to be removed. It is likely that this noise depends not only on the magnitude of the transverse motion, but on the properties of all the reflections in the sample, correlated and uncorrelated. In most cases, there is no ability to have a previous knowledge of the sample properties so a general method relies on the statistics of all the non-zero contrast pixels within the image. Any contrast pixel which is zero has had a threshold applied to it or has the entire phase error numerically removed. The remaining pixels are the data which was subject to the transverse motion, which is assumed to be experienced uniformly across the entire image. The mean μ and the standard deviation σ of the non-zero contrast pixels help to determine the contrast amount to be removed.

Using a numerical factor α , the contrast based on the statistics $\mu + \alpha\sigma$ is removed from the phase variance contrast image $C(x,z)$. Without additional processing, this method negatively affects the contrast regions which have achieved maximum phase variance contrast. With the limit imposed on phase changes of $\pm \pi$, the maximum phase variance for a random distribution is 3.3 radians^2 . Renormalizing the contrast data after removing the numerical factor gives us the adjusted contrast:

$$(C(x,z) - (\mu + \alpha\sigma)) \left(\frac{3.3}{3.3 - (\mu + \alpha\sigma)} \right) = C'(x,z) \quad (5.1)$$

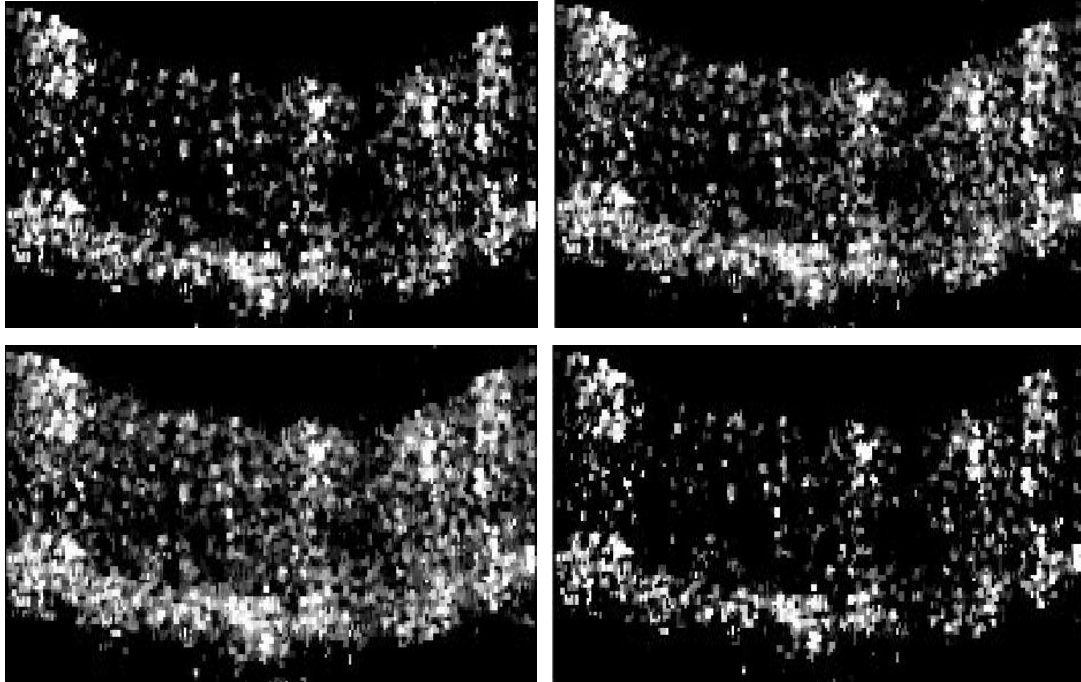


Figure 5.18: Additional noise removal method applied to the phase contrast image of Figure 5.17. The corrected contrast images are presented for the cases of $\alpha=0$ (upper left), $\alpha=-1$ (upper right), $\alpha=-2$ (lower left), and $\alpha=1$ (lower right).

The only factor left to determine is the numerical factor α , which determines how strong the contrast removal is. Altering α between -2 and 2, the decision of the optimal term to use is not well defined. With α too high too much contrast information is removed, but if α is too low then there is no apparent change. After comparing the contrast subtraction images, the case of $\alpha = 0$ was chosen for use in the contrast images.

The first comparison for this technique is between the non-corrected phase contrast image for a low transverse motion noise BM-scan and the corrected phase contrast image for a large transverse motion BM-scan. The low transverse motion noise BM-scan chosen was the same data used to create the OCT intensity image for Figure 5.17. The vessel

visualization is definitely improved compared to the non-corrected case, but there is room for improvement on this analysis method.

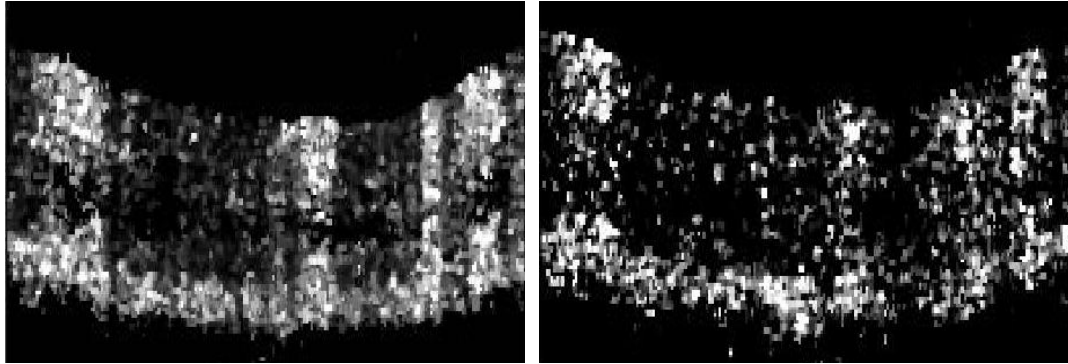


Figure 5.19: Comparison of phase contrast images between an uncorrected small transverse motion case (left) and a corrected large transverse motion case (right) with $\alpha = 0$ chosen.

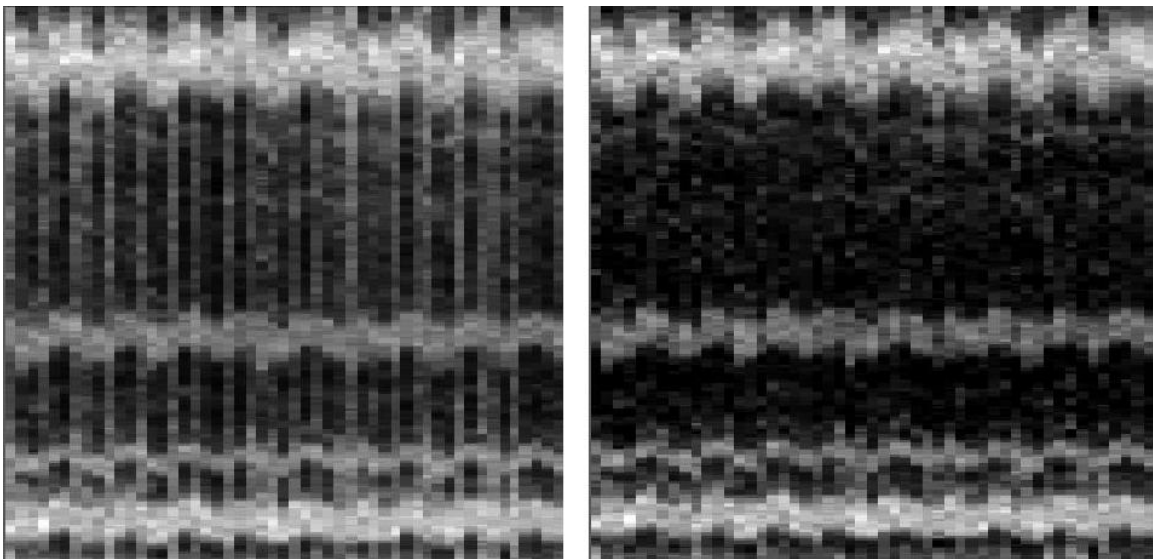


Figure 5.20: Contrast summation image over time summed over the full retinal depth, acquired over 2.6s. Images presented are before (left) and after (right) the additional motion compensation for the $\alpha = 0$ case.

Using the $\alpha = 0$ case on the en face phase contrast summation images, the improvement using this method is very obvious. The non-corrected data en face image contains vertical lines corresponding to the additional contrast motion added to the BM-scan phase variance by the transverse motion of the system, which appears to correspond to the oscillating

motion of the system. The corrected image does not appear to have any of these contrast artifacts while still experiencing the same spatial oscillations of motion due to the transverse motion.

There are limitations to using this approach to remove all of the effects of the additional transverse motion. This method makes the assumption of a primarily stationary sample. There are retinal cases in which the majority of the non-zero contrast in the image is composed of retinal flow and shadowing artifacts caused by the flow, causing this method to miscalculate the proper noise removal.

Using BM-scans acquired transversely over the retina, the transverse noise removal method is applied and the 200 x 51 transverse pixel contrast summation image was calculated. To put the contrast image into context, a 200 x 200 reflectance image created from a different buffered acquisition over the same transverse region is plotted. In this case, the noise removal technique does not remove all of the motion noise, but it is reduced for most of the BM-scans. To further improve the image quality of the contrast images, it is important to deal with the transverse motion with more than just software analysis.

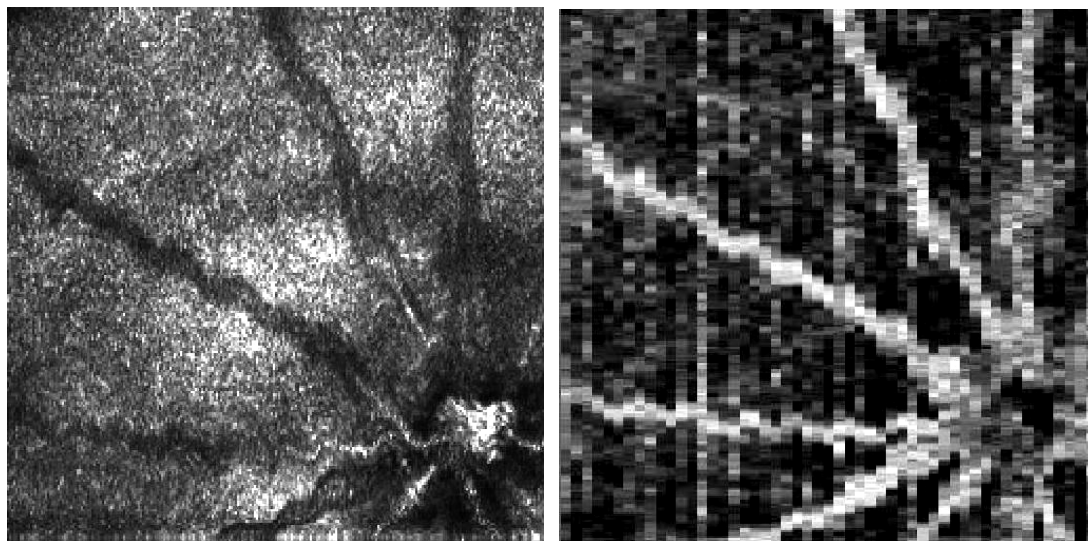


Figure 5.21: En face intensity and phase variance contrast images calculated using BM-scans and the additional noise removal method. The 200 x 200 pixel intensity image was acquired in a different buffered acquisition than the data used to calculate the 200 x 51 contrast image, but both acquisitions occurred over the same transverse scan region.

The source of the twitching of the mice was discovered to be dependant on several factors, the most important being the dosage of the anesthetic used. If the dosage was too low, the mouse would not be fully paralyzed and motion would occur over time. If the dosage was too high, there would be twitching associated with the heart beat, or due to laboured breathing. The motion due to laboured breathing also occurs when the restraints on the mouse are too tight and the airway is constricted. The ideal drug dosage of the ketamine/xylazine solution described earlier was 0.5 mL–0.6 mL for the animals used in this experiment. The animals were stable during the imaging session and also took longer to wake up afterwards. The anesthetic dosage required for each individual mouse can vary between animals, depending on several factors including the size of the animal. To properly determine the ideal dosage for future imaging sessions, a dosage response test should be performed on each animal.

5.5 En face Motion Contrast Images

With proper anesthetic dosages, the mice remained much more stationary during the data acquisition of the system. For this situation, all of the phase contrast techniques capable of 3D contrast data are reacquired to try and determine the detection limits when transverse motion is not a major concern. The first 3D phase contrast technique to re-analyze is the single scan contrast method, using 128 B-scans containing 512 A-scans each. The en face images created from the intensity, phase variance, and Doppler magnitude data use the same method as described previously. The phase variance contrast and the Doppler magnitude summation images do not have any thresholds applied before summation in this case. The Doppler shift image sums the average phase change over the entire depth of the retina. In order to avoid conflicts with the bulk motion removal algorithm, only data which has a magnitude greater than 1 radian was used within this image.

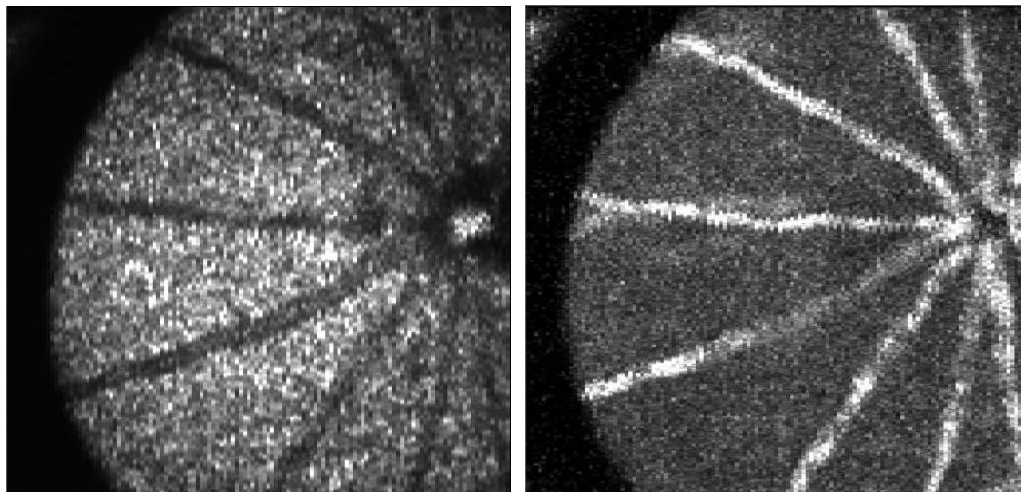


Figure 5.22 a): En face images created using 128 B-scans, each containing 512 A-scans. The intensity image (left) and the phase variance contrast image (right) sum the respective images over the entire depth of the retina.

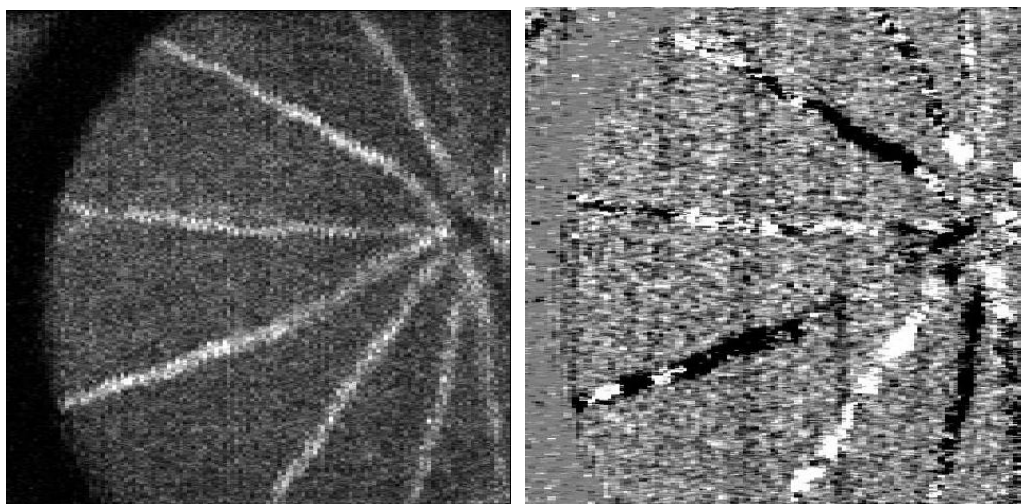


Figure 5.22 b): En face images created using 128 B-scans, each containing 512 A-scans. The Doppler magnitude image (left) sums all of the noise corrected data over the entire depth of the retina. The Doppler shift image (lower right) only sums axial flow components with a magnitude larger than 1 radian over the depth of the retina.

The conclusion for the single scan phase contrast method appears to be the same as before; the contrast analysis methods demonstrated can easily visualize the major retinal vessels with fast flow. Smaller, slower vessels and choroidal vessels do not appear to have much visualization in this method.

For the BM-scan contrast data, the intensity and phase contrast summation images were used from the same data set containing 200 x 51 transverse pixels over the retina. Although there was no obvious transverse motion occurring during the data acquisition, the phase contrast image appears to have a few locations of additional noise at random time points. The additional noise removal method was used to reduce the effect of this noise within the contrast image. Both summation images were calculated through the depth summation over the entire retina.

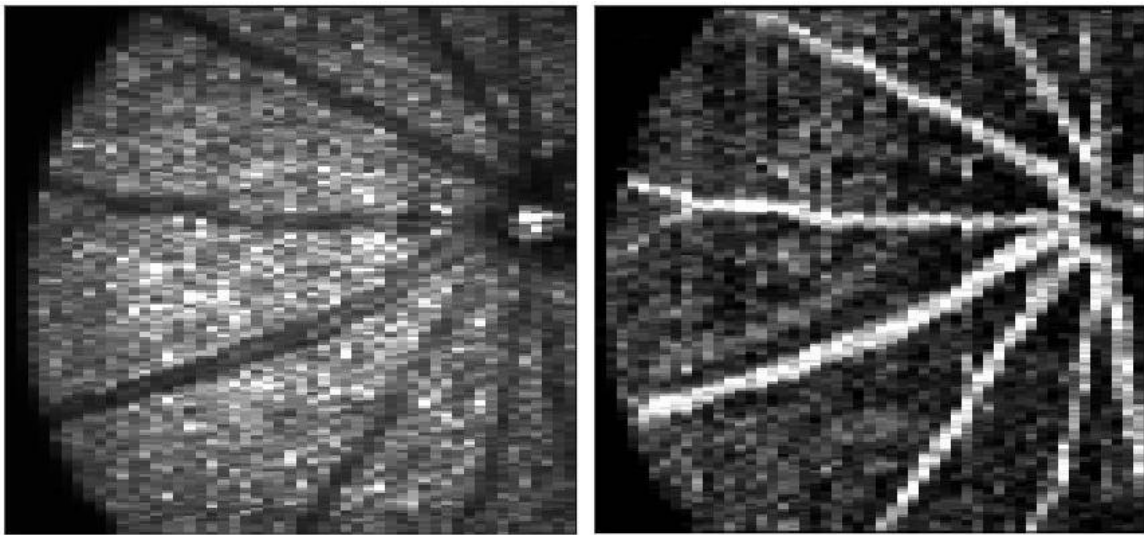


Figure 5.23: BM-scan en face intensity and phase contrast images summed over the entire retina.

To improve visualization of the smaller retinal vessels, the simplest method is to not include the choroidal vessels in the depth summation image. The problem lies in the fact that the retina is a curved surface and any chosen depth region within the retina will encounter different layers at different transverse locations. To properly isolate retinal layers of interest, the retinal image needs to be flattened.

In an ideal case, the boundaries of the retina could be automatically identified and the retina could be flattened without any assistance. Another alignment method uses cross-correlation techniques to line up successive A-scans to each other. Each aligned B-scan can be aligned to each other to flatten the entire 3D data set. Some problems arise when encountering

transverse locations with blood vessels, where the RPE and choroidal reflections can be reduced but reflection off the top of the retina is much higher than normal. Cross-correlation work can misalign the RPE of one A-scan to the top of the retina on the next A-scan. Highly absorptive regions lacking retinal layers such as the optic nerve head also provide some problems on the automatic alignment techniques. With no high-accuracy requirement of the flattening, a manual alignment of the retina was performed, accurate enough to be able to separate the contrast from the top of the retina from the choroidal motion contrast.

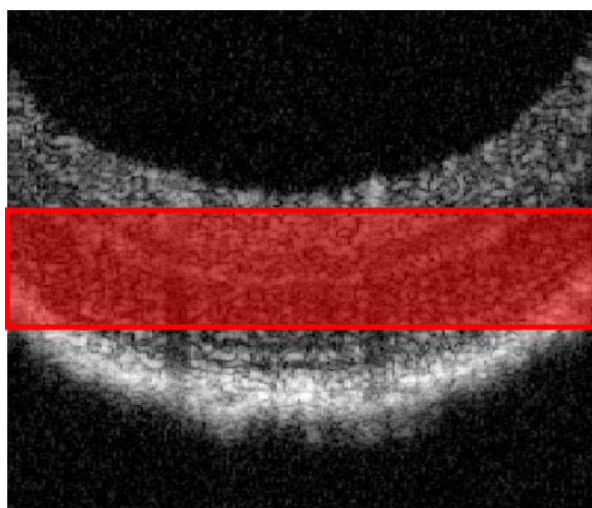


Figure 5.24: Schematic of a summation region chosen for an en face depth summation image over a curved retinal image.

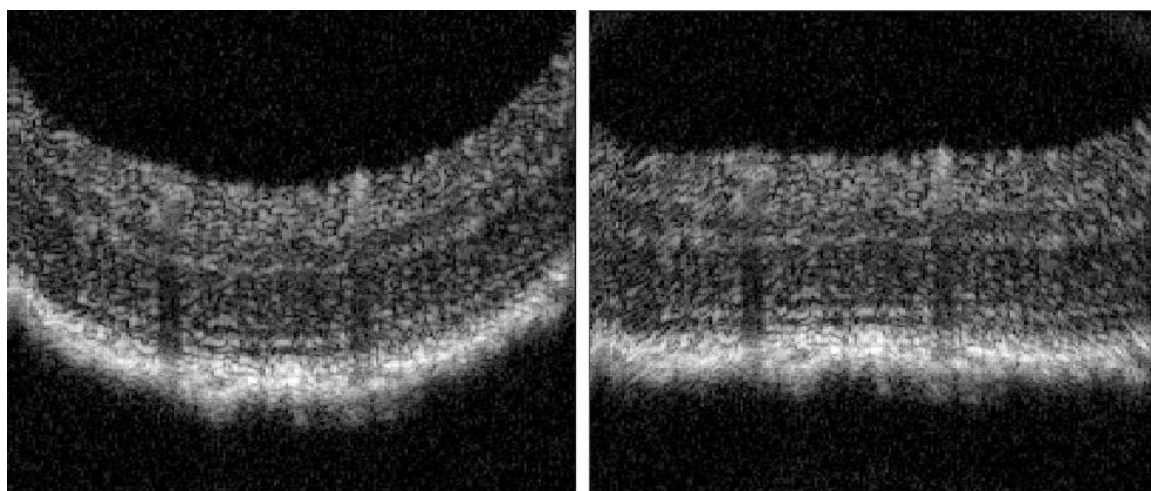


Figure 5.25: Averaged B-scan intensity image before and after realignment to flatten retina.

To observe where the motion contrast exists within the mouse retina, an overlay contrast image is produced for a flattened retinal image. While the side-by-side comparison of the averaged OCT intensity image and the phase variance contrast image provides valuable insight, combining these two images can allow for more visualization. For this demonstration, every phase variance contrast pixel with a value greater than 1 radians² will completely remove the OCT signal in the overlay image. The phase contrast image has a scale of 0 to 3 radians².

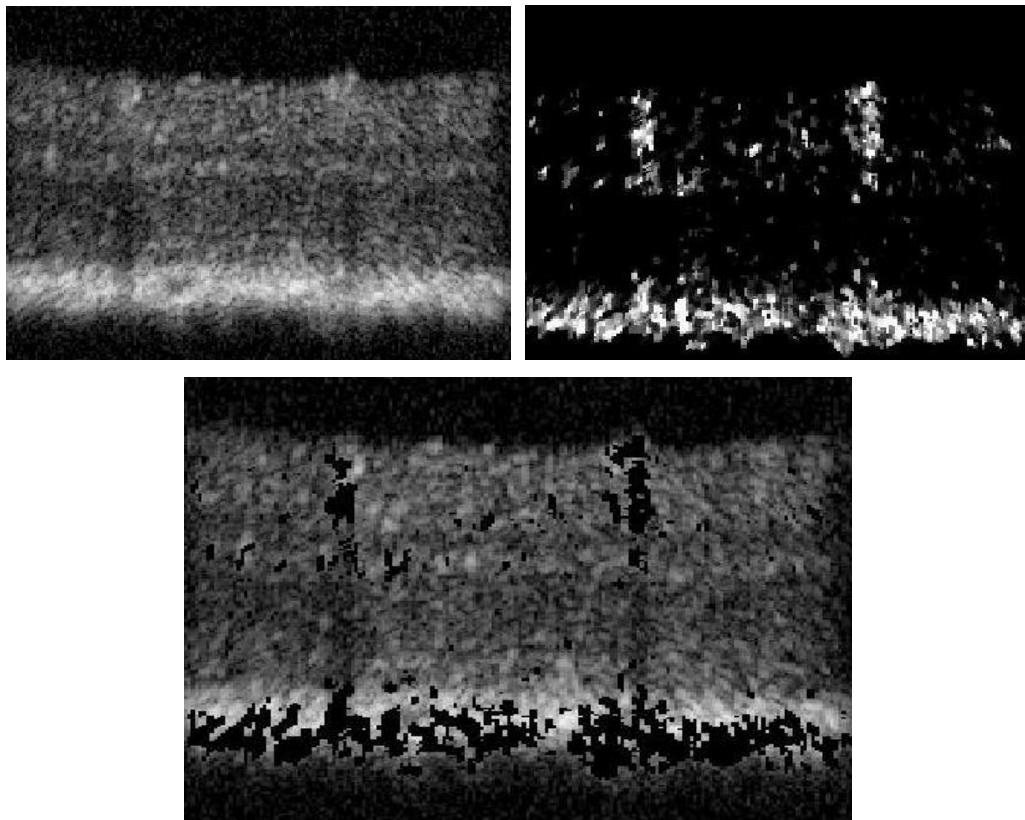


Figure 5.26: Averaged intensity image (upper left) and the phase contrast image (upper right) from a BM-scan after retinal flattening. An overlay of the phase contrast and the intensity images (bottom) was created by removing all signal from the intensity image where the phase variance contrast was greater than 1 radians².

The larger retinal vessels with the shadowing of contrast are observed in the retina as well as some smaller regions of contrast which might be associated with smaller retinal vessels. More information is required to determine whether they are true motion or just artifacts.

While it is not possible to separate out the choroid and RPE regions on the intensity image for the mouse retina in this system, the relatively static regions of the RPE can be observed above the motion of the choroidal vessels in the overlay image.

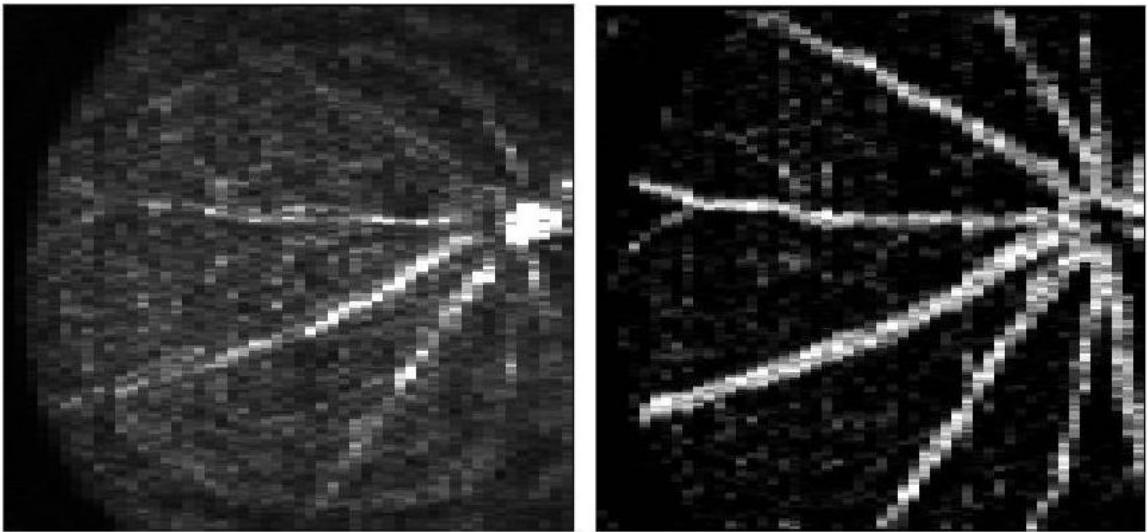


Figure 5.27: En face summation images of the intensity (left) and the phase variance contrast (right), with summation chosen to be over only the top half of the retina.

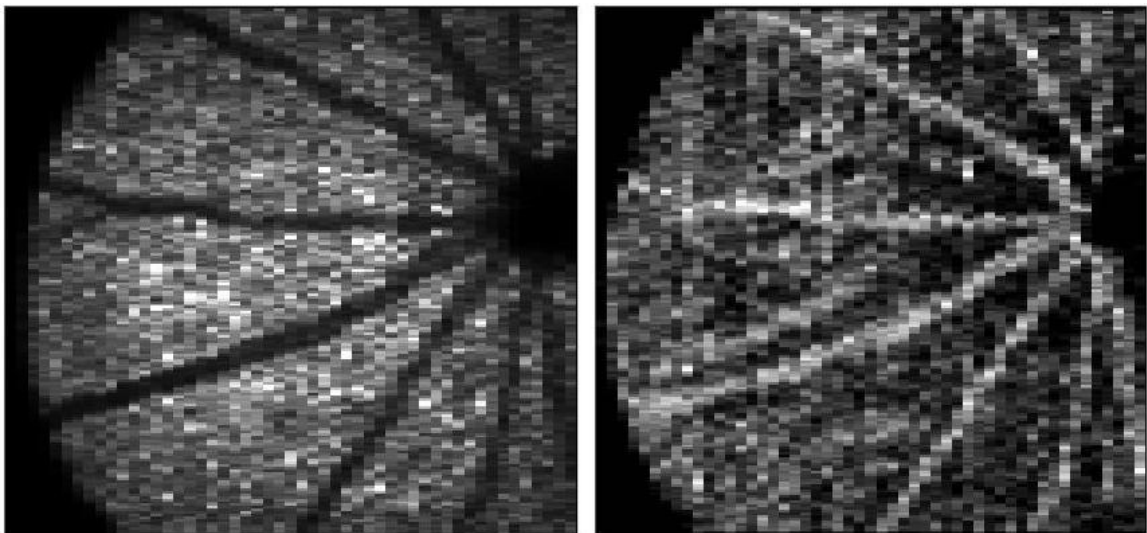


Figure 5.28: En face depth summation images of the intensity (left) and the phase variance contrast (right), summed over the bottom half (choroidal region) of the retina.

En face summation images were created using the flattened retinal data to create intensity and phase contrast images for the top half of the retina as well as images for the choroidal regions of the retina. With the RPE reflection removed, the primary reflection observed for the top half of the retinal intensity image comes from the top of the blood vessels near the optic nerve head. The choroidal region intensity image observes the expected RPE reflection overlapped with the blood absorption of the major retinal blood vessels in the eye.

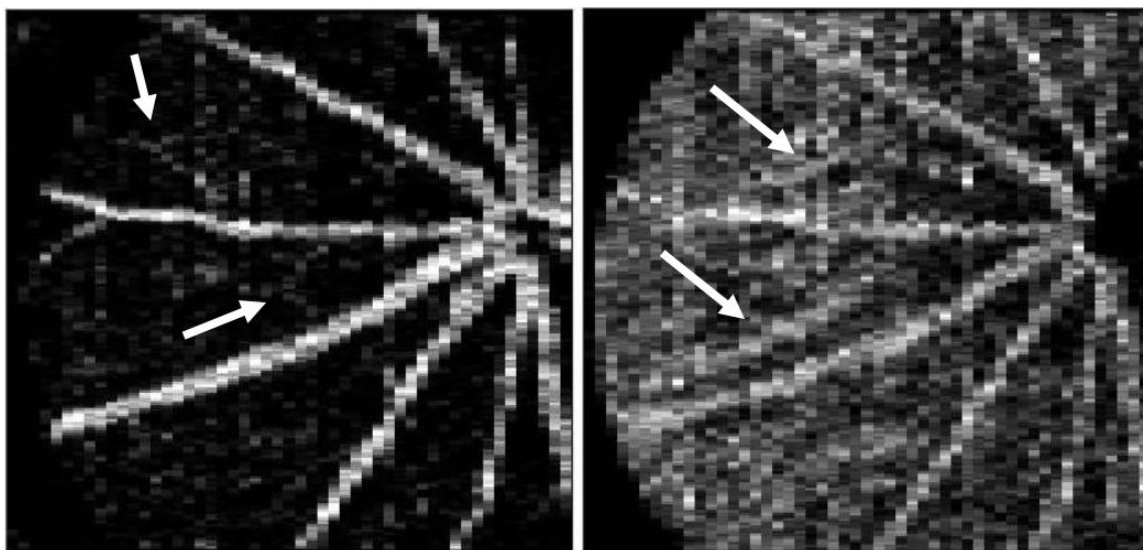


Figure 5.29: Comparison of en face phase variance contrast images with different summation regions of the same data. The contrast images correspond to the surface retinal vessels (left) and the choroidal vessels (right) as well as the shadowing contrast of the major retinal vessels. Arrows correspond to locations of identified blood vessels not present in the comparison image.

The separation of the en face phase variance contrast images for the different depths allows visualization of vessels that may not have been identified with the full depth summation. The summation image over the top of the retina observes small vasculature connected to the major retinal vessels which were not visible in the full summation image. The choroidal region contrast image contains a portion of the shadowed motion contrast due to the major retinal vessels above those locations, but there are several vessels that can be identified in addition which are located only within the choroidal region. These are major choroidal vessels located within the mouse eye. With the identification of choroidal vessels and tiny

vasculature, there appears to be potential for the BM-scan to be used to detect CNV in retinal imaging situations. There is still room for improvement for this data acquisition method to be able to improve the visualization of the tiniest vessels in the eye.

Fluorescein angiography is the gold standard of visualizing vasculature in the retina. The expected vasculature in the mouse retina using this technique is much more substantial than visualized with the retinal phase contrast summation image of Figure 5.29 [6,7]. If we assume that the smallest retinal vessels observed act like the segmental vessels of the zebrafish, blood passes through them only a fraction of the total time. Fluorescein angiography utilizes a CCD camera to take the picture of the fluorescence over the integration time, resulting in a measure of the average blood over the integration time for the fundus of the eye. Thinner blood vessels containing blood only a fraction of the time will appear much less bright in the angiography image than the major blood vessels which saturate the image, which is the case for the demonstrated image. With an understanding of the smallest vessels, the OCT phase contrast images can be improved to obtain the same visualization.

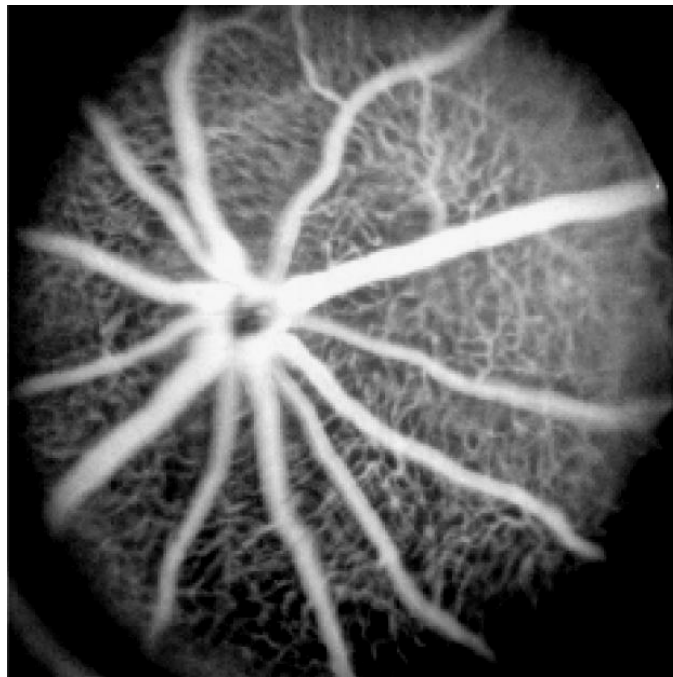


Figure 5.30: Fluorescein angiography image of mouse retina. Image reproduced from [7].

5.6 Improving BM-scan Capabilities

With the assumption that the smallest vessels in the eye act like the segmental vessels in the zebrafish, there is a limit to the vascular visualization that can occur in a single contrast image. If the blood is not located within the vessel when the image is taken, there is no contrast to be obtained. Statistically, for any given phase contrast image acquired for the retina, there will be regions of vasculature which do not contain any blood or motion contrast at all. This is not a problem with the increase of statistics; with multiple images taken over the same location, the chances of imaging a region when blood is present increases. To reduce the alignment requirements for multiple contrast images taken over several buffered acquisitions, the BM-scan is optimized by maximizing the statistics for the memory buffer of the system through repeating the contrast measurements within one buffered acquisition.

With an improvement to the acquisition computer memory to 2 GB, the maximum buffered acquisition is approximately 512 x 256 total A-scans. The optimized BM-scan parameters use a 100 transverse pixel B-scan with an x-scan duty cycle of approximately 80%, 5 B-scans for each BM-scan, 50 transverse pixels in the y-scan direction and repeated 4 times. The y-scan duty cycle in this case is approximately 98%. The resulting acquisition is a BM-scan phase contrast transverse scan region of 100 x 50 pixels, repeated 4 times. The time between phase measurements for the BM-scan in this case is 5 ms and the time between each of the 3D BM-scan data sets is 1.3 s.

With smaller transverse pixel numbers for the BM-scan and faster fly-back speeds required of the scanners, a smaller image scan range is required. For the 100 transverse pixel BM-scan, the scan range in each direction was chosen to be less than 1 mm. The exact size of the image depends on the optical alignment of the system at the time of the data acquisition. In order to compare the results of the repeated 100 transverse pixel BM-scan to previous techniques, the previously defined 200 transverse pixel BM-scan was used to image over the same transverse scan region extending over less than 1 mm for each scan direction.

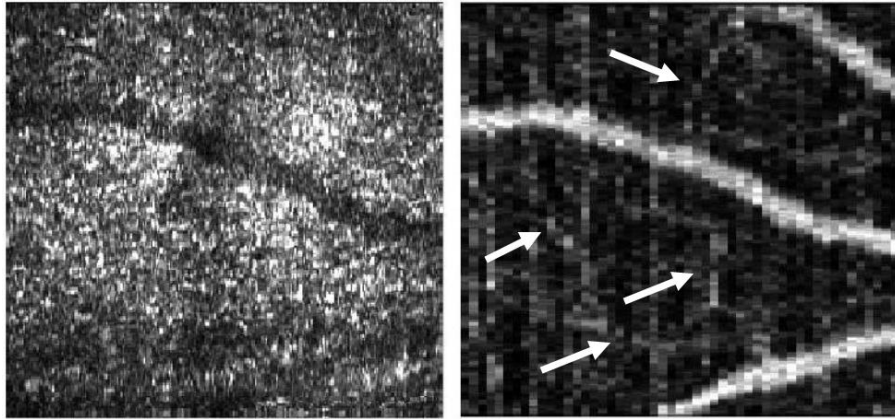


Figure 5.31: BM-scan en face summation images of intensity (left) and phase variance contrast (right). The intensity image was summed over the entire retina, while the contrast image was summed over the top half of the retina for the 200 transverse pixel BM-scan data across retina. Arrows identify some of the smaller visible blood vessels.

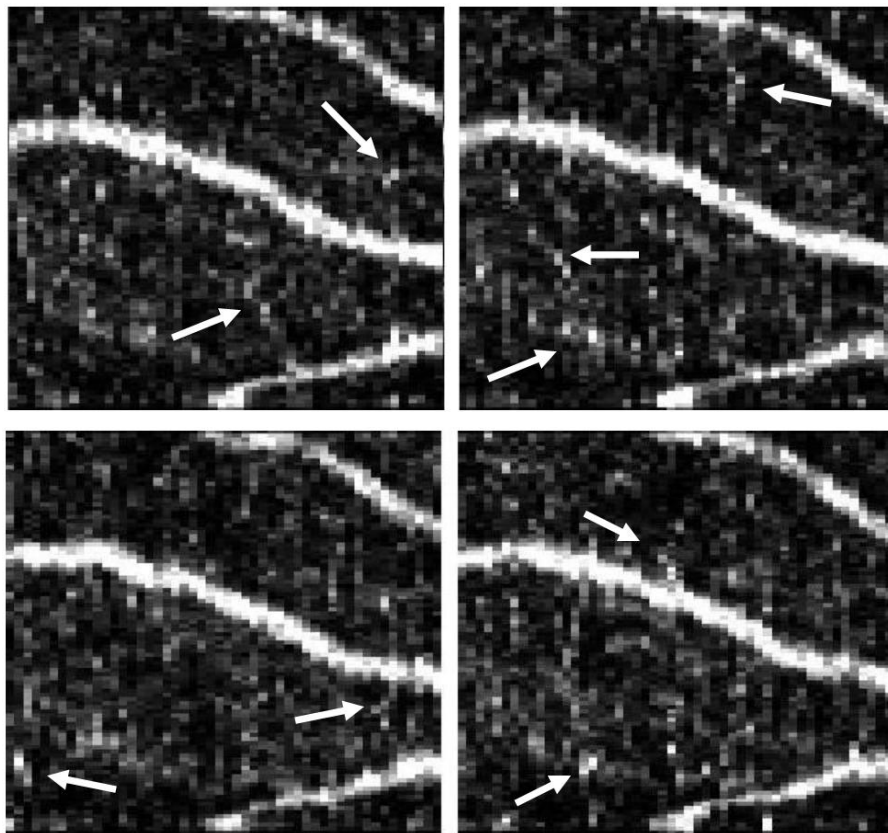


Figure 5.32: En face phase contrast summation images created from the top of the retinal data acquired from the repeating 100 transverse pixel BM-scan method. Arrows identify vascular events not visualized within all four contrast images. Transverse scan region of image is identical to Figure 5.31.

The BM-scan data acquired in both the 200 transverse pixel case and the repeating 100 transverse pixel case can visualize the smaller retinal vessels of interest. Within the five different contrast images, there were different regions of the vasculature that were able to be identified as expected for randomized flow within the vessels. To combine the visualization capabilities of the individual contrast images, the four 100 transverse pixel BM-scan contrast images were averaged without any transverse realignment. To improve the contrast of the image, the data was gamma corrected using $\gamma = 0.85$. For an intensity image $I(x,y)$ with a maximum defined as I_0 , the gamma corrected image is of the form:

$$I'(x,y) = I_0 \left(\frac{I(x,y)}{I_0} \right)^\gamma. \quad (5.2)$$

The averaging technique of the four individual contrast images was repeated for the phase contrast summation over the entire retina.

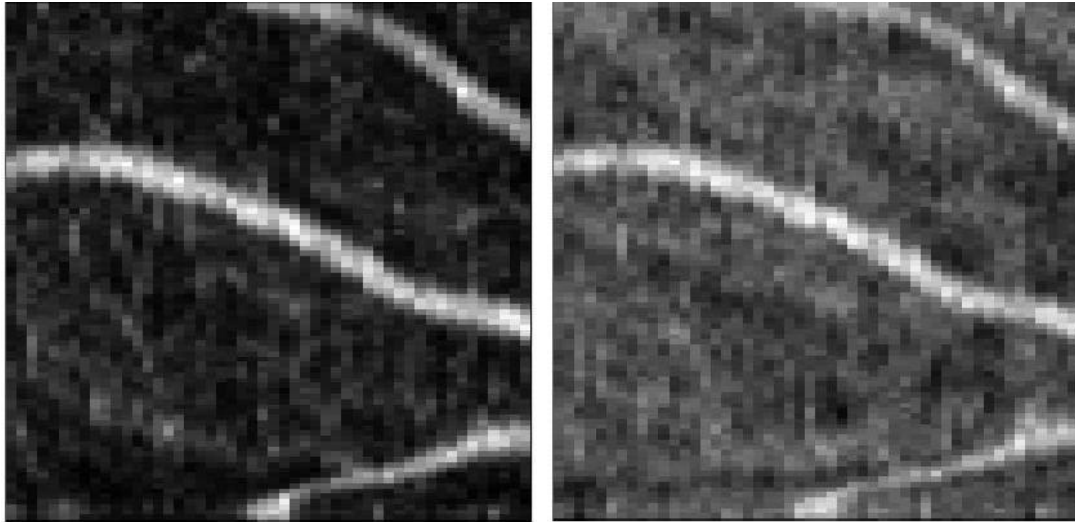


Figure 5.33: Mean en face contrast images from the repeating BM-scan method. The images created were for the top half of the retina (left) as well as the full retinal summation (right). Each image was gamma corrected to improve visualization of the weaker contrast regions.

In many cases, there may be transverse sample motion occurring during the data acquisition of the BM-scans. For this situation, vertical contrast lines may appear in the

phase variance contrast image that can obfuscate the vascular visualization. If two different buffered acquisitions were acquired successively but with the primary scan direction in perpendicular directions, the contrast lines due to transverse motion will occur in two different directions. These two images could be aligned and analyzed to allow improved vascular visualization.

Two sequential buffered acquisitions were taken using the repeating 100 transverse pixel BM-scan method, each with a primary transverse scan direction perpendicular to each other. In order to properly compare the images, the phase contrast summation images for the top of the retina were extrapolated into 100 x 100 pixel images. To improve visualization of the lower signal from the small vessels, the scale of the image was set to 75% of the same data in Figure 5.33.

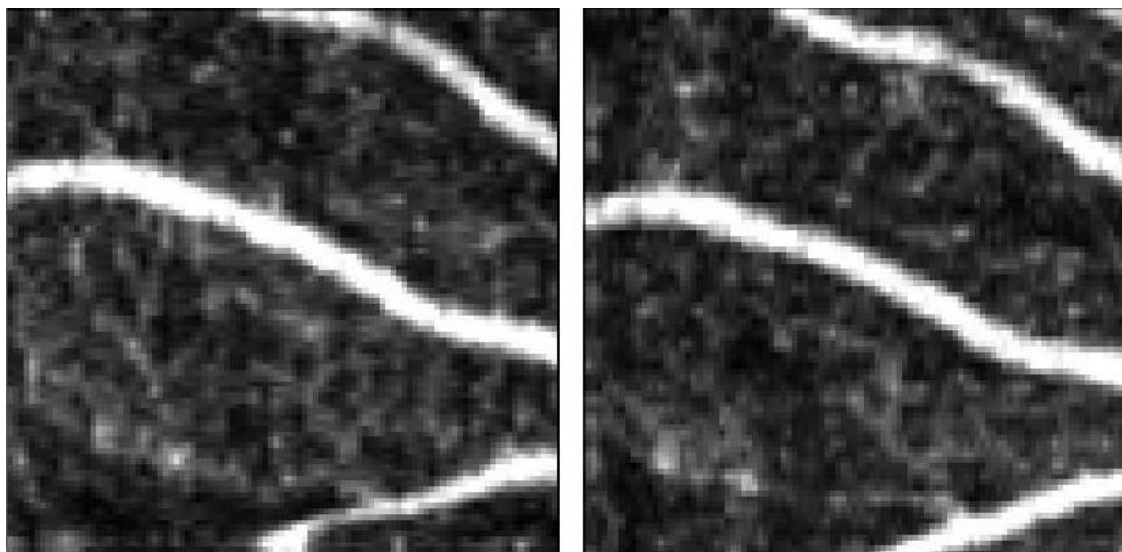


Figure 5.34: Mean contrast summation images from two different acquisitions of the repeating BM-scan method, summed over the top half of the retina. Images were acquired with perpendicular primary transverse scan directions. Images were extrapolated to the size of 100 x 100 pixel for comparison.

Aligning these two images to each other removes the motion between successive buffered acquisitions and takes the mean results in the image of Figure 5.35.

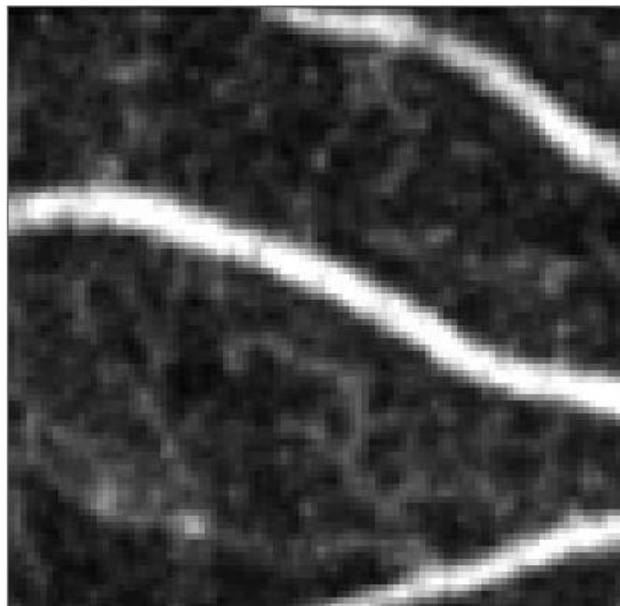


Figure 5.35: Mean of the two different mean en face contrast images of Figure 5.34 after transverse alignment.

The image in Figure 5.35 is basically the mean contrast from 8 different phase contrast summation calculations, trying to reduce the possible noise in the system while improving the vascular visualization. To adequately compare how well this technique visualizes vasculature, it needs to be placed side-by-side to the expected vasculature of the fluorescein angiography image of Figure 5.30, scaled to approximately the same size. Both images are taken from completely different mice and locations within the retina, so an exact comparison of specific vessels is not possible.

It needs to be noted that a direct comparison between the two images is not completely appropriate. Fluorescein angiography images are a gauge of the average blood occupying the transverse location at a given time, which is dependent on the thickness of the blood vessels. The mean phase contrast summation image also is dependent on the thickness of the blood vessel which is summed over, but the larger vessels also contain shadowing contrast which increases their contrast in comparison. Also, the contrast within the vessels in this case depends partially on the flow velocity properties, which can further reduce the relative contrast between the larger fast blood vessels and the smaller vasculature. The comparison that should be made between the averaged phase contrast summation image

and the fluorescein angiogram is the ability of both to observe the smallest vessels expected within the retina.

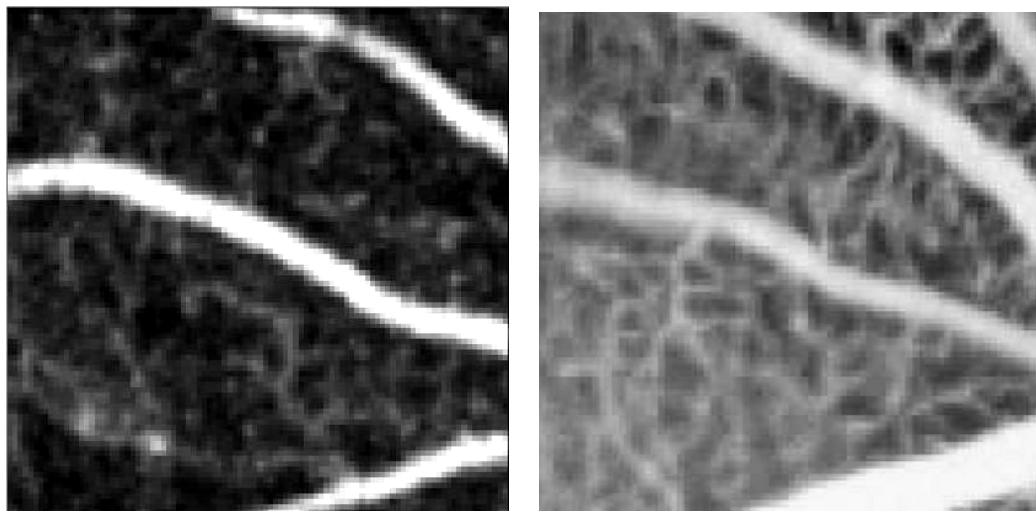


Figure 5.36: Comparison of the averaged phase contrast image to the expected form of fluorescein angiography. The phase contrast image, taken over the top half of the mouse retina presented in Figure 5.35 is compared to the angiography image of Figure 5.30, zoomed in to approximate a similar region of the mouse eye.

The contrast image presented in Figure 5.35 is just one possible form of analysis of what can be referred to as the 4D phase contrast data; 3D phase variance contrast information acquired repeatedly over time. Each stage in the image calculation uses a mean calculation: each en face contrast summation image is essentially a representation of the mean contrast over the chosen depth slice in the image, the mean contrast was calculated from all four en face images created from one buffered acquisition, and the two independent mean contrast images were aligned and averaged to create the final contrast image.

There are many other types of analysis that can be performed on the phase contrast data. If the final contrast image was created by using the maximum value of all of the individual contrast images, the signal from all the vasculature regions could be improved. Unfortunately, the maximum method would amplify the noise of any one image within the analyzed set. With any analysis technique, there is a tradeoff which comes from trying to separate the signal and noise when they are very similar. By trying to amplify the weak

contrast signal from regions, the noise of the image can be similarly amplified. By trying to exclude the noise terms from the contrast image, actual motion contrast signal can be lost due to the similarity.

For the small vascular regions, the contrast is very similar to noise. When flow occurs within the vessel during the imaging session, contrast is observed; otherwise, any possible contrast is obfuscated by the noise analysis of the image processing. Since the time in which flow occurs is random, the contrast observed for a flow location is also random in time, making it hard to distinguish from simply noise. Assuming that the contrast associated with flow from a vessel appears as a spatially localized pocket of high contrast, another form of analysis was used to isolate these regions from the weaker but spatially larger regions of noise which would create comparable summation image intensities. For a chosen depth region typically used for a contrast summation, a smaller window of approximately $20\ \mu\text{m}$ was chosen to slide across the entire depth region, performing summations over the depth locations identified by the sliding window. The maximum summation within the depth region was used as the en face contrast image pixel.

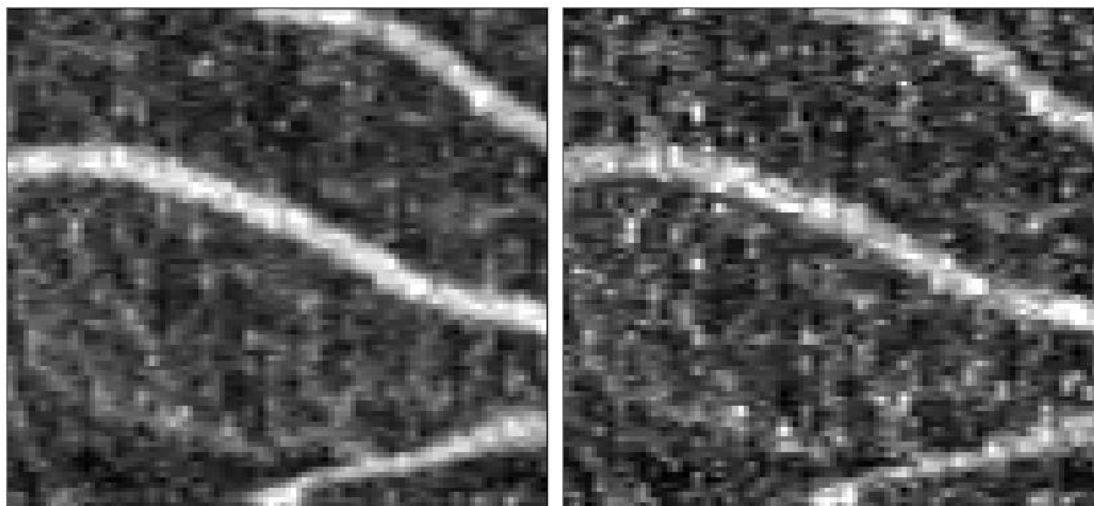


Figure 5.37: En face contrast summation images for the sliding window technique of $20\ \mu\text{m}$ were calculated for the repeating BM-scan phase contrast data. The mean (left) and the maximum (right) of the four individual contrast images was calculated for the data set. Both images were gamma corrected and extrapolated to 100×100 pixels.

The sliding window technique was used on the repeating BM-scan phase contrast data to identify the largest localized contrast within the depth region and create en face images with these results. To allow multiple analysis techniques to be used, the mean and the maximum image of the four en face images within the buffered acquisition were calculated and presented in Figure 5.37. Both analysis techniques have definite visualization benefits, identifying potential vascularization regions not clearly visible in the other image. The data used for analysis and the depth region chosen was identical to the left image of Figure 5.34, allowing for a direct comparison of the analysis techniques for the same data.

With the demonstration of vascular visualization and all of the information available with the 4D phase contrast data set, there is a lot of potential of contrast improvements. With the available 3D contrast information, these techniques can develop into a form of 3D fluorescein angiography, which can be useful for a whole range of ophthalmic diagnostics beyond just AMD. For this to happen, one of the most important required factors is the ability to identify vascular contrast regions from a single 2D phase contrast image. The main problem in many images is the inability to identify contrast regions as sample motion contrast or simply contrast noise that needs to be removed. Further work and analysis will allow more properties of the vascular contrast regions to be identified for easier extraction, which results in improved visualization of the vascularization.

5.7 Discussions of Human Imaging

The phase contrast demonstrations of mouse retinal vascular imaging demonstrate the potential of these techniques for future ophthalmic diagnostics. While further study in mouse retinas may help the understanding of the contrast images and the noise experienced in the images, there are no experimental reasons to not move these contrast techniques into human retinal imaging. Safety standards have been in place for a long time with this technology and it will be very useful to determine how well these contrast methods can image the intended ocular disease symptoms (like leaking neovascularization).

The human retina, as opposed to the mouse retina, has many fairly well identified layers around the RPE and choroidal region. Even the rat has a more distinguished layering for the RPE and choroid compared to the mouse [4], even with a very high axial resolution. With the lack of separation observed between the RPE reflection and the choroidal reflections, the overlay of contrast and intensity images of Figure 5.26 is the only suggestion of two distinct regions. Human retinas will allow the confirmation that the regional difference in contrast observed is actually between the choroidal flow and the relatively static RPE.

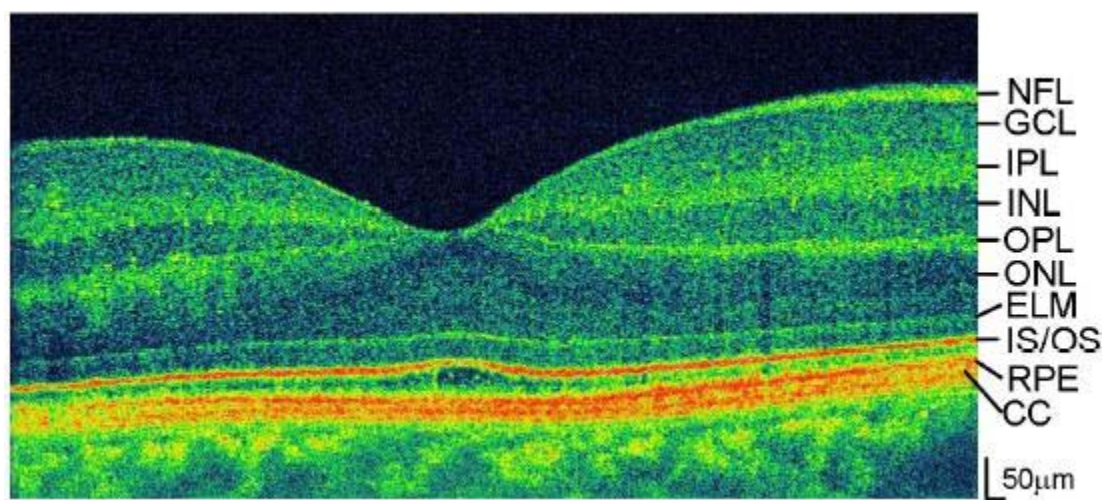


Figure 5.38: High density human retinal B-scan images created from 3000 A-scans across approximately 2.5 mm over the fovea. The image was reproduced from [8]. Axial resolution in tissue is approximately 2 µm for the imaging system.

Human retinal imaging also incorporates the ideal scenario for testing phase noise analysis and removal techniques which only comes from eyes containing high visual resolution: the blood vessel-free region of the fovea. By imaging healthy eyes, the region of the fovea provides the perfect negative control; any contrast observed in this region above the choroid is due to uncompensated phase error, transverse motion occurring of the sample, or some other effect which has not currently been considered. These images can be acquired simultaneously with the neighbouring regions which contain a well defined vascular structure, as demonstrated with fluorescein angiography.

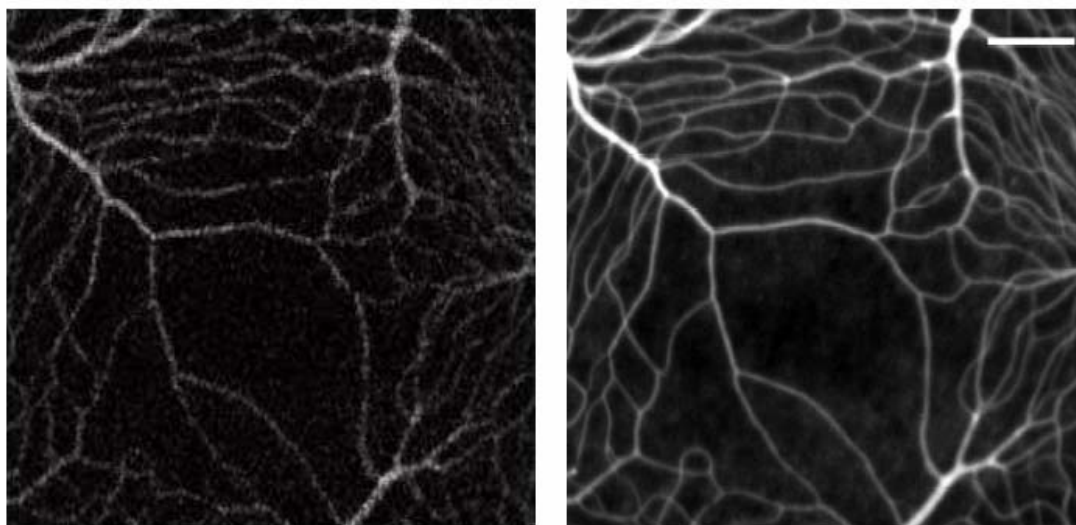


Figure 5.39: Fluorescein angiography images of monkey retina acquired with a high resolution high speed camera. A single frame of the camera (left) is compared to an image averaged from more than 1000 aligned images. Image reproduced from [9]. Scale bar on averaged image is 150 μm .

Fluorescein angiography of the monkey retina demonstrates a vascular structure very comparable to human retinas. The presented images are a single frame of the high speed camera in the system and the image after transverse motion alignment and averaging of more than 1000 separate frames from the camera. The foveal avascular zone in the center of the image is surrounded by a complete capillary bed. The small fluorescein signal observed around foveal region in Figure 5.39 is likely a fraction of the choroidal vascularization, not easily observed with fluorescein imaging due to the absorption of the light by the RPE.

The single frame of the angiography image is a great example of what might occur for the ideal case of a single en face contrast summation image in the retina. The major blood vessels surrounding the fovea have contrast in the vasculature, but the blood is not in all regions for any given time point. The faint fluorescein signal observed in the averaged image, which might be choroidal flow, is not observed at all within a single angiography image from the high speed camera. With additional noise, the single camera image would also have a hard time observing some regions of the vasculature with the finer structure,

making a situation very similar to the introduction of phase noise to the en face contrast image. With improvements to the analysis techniques, the phase contrast methods demonstrated for SDOCT have the potential to not only mimic the imaging capabilities of fluorescein angiography but add additional information not available with the previous technique.

5.8 References

1. E. Garcia de la Cera et al., "Optical aberrations in the mouse eye," *Vision Research* 46, 2546 (2006).
2. M. Paques et al., "High resolution fundus imaging by confocal scanning laser ophthalmology in the mouse," *Vision Research* 46, 1336 (2006).
3. "Cell tracking using SLO angiography – Bio-Medical Physics & Bio-Engineering, University of Aberdeen," <http://www.biomed.abdn.ac.uk/Abstracts/A00665/>.
4. V. Srinivasan et al., "Noninvasive Volumetric Imaging and Morphometry of the Rodent Retina with High Speed, Ultrahigh-Resolution Optical Coherence Tomography," *Invest. Ophthalmol. Vis. Sci.* 47, 5522 (2006).
5. S. Makita et al., "Optical Coherence Angiography," *Opt. Express* 14, 7821 (2006). <http://www.opticsexpress.org/abstract.cfm?id=97672>.
6. R. D'Amato et al., "Microscopic Visualization of the Retina by Angiography with High-Molecular-Weight Fluorescein-Labeled Dextran in the Mouse," *Microvascular Research* 46, 135 (1993).
7. N.L. Hawes et al., "Mouse fundus photography and angiography: A catalogue of normal and mutant phenotypes," *Molecular Vision* 5, 22 (1999).
8. M. Wojtkowski et al., "Ultrahigh-resolution, high-speed, Fourier domain optical coherence tomography and methods for dispersion compensation," *Opt. Express* 12, 2404 (2004). <http://www.opticsexpress.org/abstract.cfm?id=80147>.
9. D.C. Gray et al., "In vivo fluorescence imaging of primate retinal ganglion cells and retinal pigment epithelial cells," *Opt. Express* 14, 7144 (2006). <http://www.opticsexpress.org/abstract.cfm?id=96196>.